# Frequency analysis of reset systems containing a Clegg integrator

An introduction to higher order sinusoidal input describing functions

Kars Heinen

Master of Science Thesis

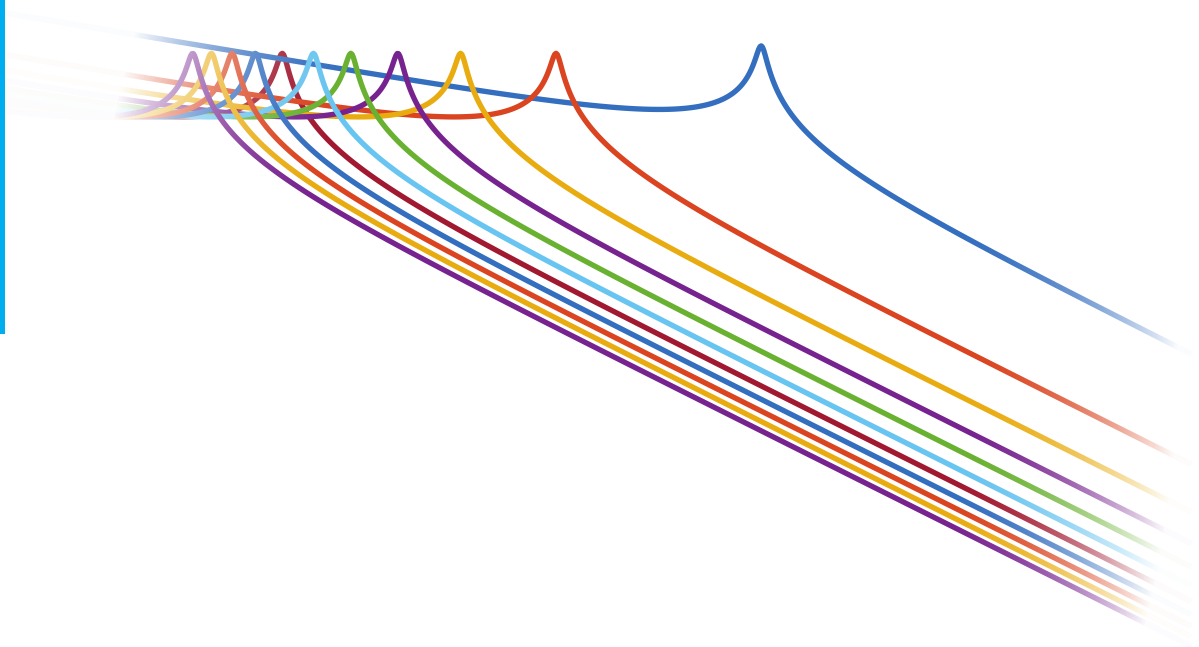

TU Delft Delft University of Technology

Delft Center for Systems and Control

# Frequency analysis of reset systems containing a Clegg integrator

## Introduction to higher order sinusoidal input describing functions

Master of Science Thesis

For the degree of Master of Science in Systems and Control at Delft University of Technology

Kars Heinen

May 15, 2018


| | | |
|---|---|---|
| Student number: | 4091485 | |
| Thesis committee: | prof. dr. ir. J.W. Van Wingerden | TU Delft, chairman |
| | Dr. S.H. HosseinNia | TU Delft, supervisor |
| | Dr. N. Saikumar | TU Delft, co-supervisor |
| | ir. A. Zondervan | Hittech Multin, supervisor |

Faculty of Mechanical, Maritime and Materials Engineering (3mE) · Delft University of Technology

The work in this thesis was supported by Hittech Multin B.V. Their cooperation is hereby gratefully acknowledged.

# Abstract

PID is the most popular controller in the industry. PID controllers are linear, and thus have fundamental limitations, such that certain performance criteria cannot be achieved. To overcome these limitations, nonlinear reset control can be used. Reset control can achieve less overshoot and a faster response time than linear controllers. However, the resetting mechanism has a jump function which causes jumps in the control input, which can result in limit cycles.

Linear filters and controllers are designed in the industry using loop shaping, which is done in the frequency domain. In this thesis it is investigated how to analyze reset systems in the frequency domain. A reset system is nonlinear, so transfer functions needs to be approximated by describing functions. The sinusoidal input describing function considers only the first harmonic of the output and therefore does not capture all the dynamics of the element.

The effects of the higher order harmonics are important in precision systems, since unwanted dynamics should not be excited nor should performance be affected. In this thesis, the higher order sinusoidal input describing functions (HOSIDF) are derived analytically. The HOSIDF shows the magnitude and phase response per harmonic, such that stability and performance analysis can be improved.

Because the HOSIDF shows multiple responses, it is not trivial how to do loop shaping. The information from the HOSIDF is combined, creating a combined magnitude and combined phase response. It is seen that the combined magnitude looks promising, but the combined phase has jumps. It is concluded that the combined magnitude and combined phase are not mature enough to rely on during loop shaping and further work in this direction is required.

# Table of Contents

# List of Figures

# List of Tables

# Preface and Acknowledgments

This report is my master thesis of the MSc Systems and Control at the Delft Center for Systems and Control (DCSC) department of the TU Delft. This project is done at a different department: the Precision and Microsystems Engineering (PME) department of the TU Delft. In February 2017, I was looking for a graduation project at the PME department of the TU Delft. After some talks with Hassan, an internship/graduation project at Hittech Multin B.V. was proposed. The internship was about implementing several controller blocks for one of their demonstrator setups. After the internship, I stayed with the company to work on a graduation project.

Hittech Multin and the TU Delft are collaborating to design and implement complex order control, which is reset control combined with fractional order control. This new type of control got my attention, because it can overcome fundamental limitations of linear controllers.

I would like to thank my supervisors for their time and support throughout my thesis. From the PME department, I'm supervised by Hassan and Niranjan. Thank you for all the enthusiasm during my work and always making some time to help me out. From the DCSC department, I was supervised by dr. ir. Wouter Wolfslag. Wouter, thank you for the feedback on my report and the tips and tricks to write better. Too bad you couldn't be part of my committee anymore, I wish you all the best in Scotland! From the company, I'm supervised by Arnold. Arnold, thank you for the discussions we've had and all the tips and tricks to get through my graduation project. I've tried my best to keep the lawn tidy and trim the grass blades.

# Chapter 1

# Introduction

PID controllers are one of the most used controllers in the industry [4]. Their structure is simple, they are easy to implement and easy to tune. Because they are linear controllers, they have fundamental limitations. When designing high precision mechatronic systems, performance is often limited because of these limitations.

These limitations could be avoided by introducing more advanced controllers. However, introducing other types of control is hard to push to the industry, because often they are too complex, require a lot of computational power or require a good model of the plant. Industry wants better control, but at the same time wants the simplicity of PID control. It is impossible to improve PID control beyond its linear limitations, and hence non linear behavior needs to be implemented.

PID control consist of three gains; the proportional gain (P), the integrator gain (I) and the derivative gain (D). Non linear control dynamics can be implement for all three terms. The P term of PID can be improved by introducing e.q. variable gain methods, as has been investigated by [5]. Variable gain considers only the P action in PID, which has no influence on the phase of the system. The D term of PID creates phase lead, but also introduces unwanted gain in the system. The D term can be improved by split path non linear (SPAN) filters, as seen in [6]. In [6], phase lead is created without increasing the gain. The SPAN filter however does not fit easily in the PID framework, because it depends on the input amplitude as well, making frequency analysis not sufficient anymore. The I term of PID creates high gain at low frequencies, but introduces unwanted phase lag. Reset control can improve the I term, by reducing its phase lag. Reset control is easily implemented in the PID framework, because only the integrator element is replaced. Because of its easy implementation, reset control is studied in this thesis.

A reset system contains a Clegg integrator instead of a linear integrator. The Clegg integrator was introduced in the 1950s by J.C. Clegg [7]. This integrator can reset its state and thus has nonlinear behavior. The Clegg integrator has only approximately -38° phase lag but similar gain behavior compared to a linear integrator. It is this property that is interesting, because it breaks Bode's phase gain relation [8]. The phase lead could reduce overshoot and improve

settling time. Qualitative design of reset control was introduced in the 1970s, where Horowitz did pioneering research about the Clegg integrator used in control system design [9].

Linear controllers and filters are designed in the frequency domain using loop shaping. Loop shaping is only accurate for linear systems, because the exact frequency response of these systems are known. To do loop shaping with reset systems, their frequency response needs to be approximated. In current literature [10, 11, 12], first order describing functions are used to represent reset systems in the frequency domain. First order describing functions are not accurate enough to cover all the dynamics. Higher order harmonics are neglected, which may contain useful information. In this thesis, the higher order harmonics are investigated. To do so, a research goal is set:

*Integrate higher order information into a frequency domain representation for the analysis of reset systems containing a Clegg integrator.*

Some subgoals are set to reach this goal:

- Show that the current frequency analysis of reset systems is not accurate enough.
- Derive analytically the higher order describing functions for a reset system.
- Visualize the higher order describing functions.
- Combine the higher order describing functions to enable loop shaping.

In the second chapter of this thesis, background theory is given on how to design linear controllers using loop shaping. In this chapter we also motivate the need to study reset systems by providing examples of the limitations of linear controllers. In the third chapter, reset systems are introduced. This is done in the time domain, as this is the natural domain to define reset systems. In the fourth chapter, the current method of analyzing reset systems in the frequency domain is discussed. This analysis is done using first order describing functions. This chapter will show why the first order describing function is not accurate enough. In the fifth chapter, the higher order sinusoidal input describing functions (HOSIDF) are derived analytically for reset systems. The HOSIDF is visualized like a describing function, showing magnitude and phase behavior per harmonic. Because the HOSIDF shows multiple responses, it is not trivial how to do loop shaping. In the sixth chapter, a new method for analyzing magnitude and phase behavior is provided, by combining the HOSIDF to form a single response. With this single response, loop shaping can be achieved.

# Chapter 2

# Background information

In this chapter, background theory is given on how to design linear controllers in the frequency domain using loop shaping. Linear controllers have fundamental limitations, of which two of them are discussed. These fundamental limitations will lead to the study of reset systems.

## 2-1 Feedback systems

When a plant needs to be driven to a certain output, a controller is used. The plant and the controller combined form a system. In practice, a system is influenced by noises and disturbances. It is desired to let the controller compensate for these disturbances and noises as well.

A general feedback system overview is given in Figure 2-1, where $P(s)$ is the plant that needs to be driven, $C(s)$ is the feedback controller, $r$ is the reference value, $d$ is the load disturbance noise and $n$ is the output noise. The load disturbance noise $d$ represents the noise that drives the system away from its reference. The sensed output is affected by noise signal $n$, which consists of measurement errors.

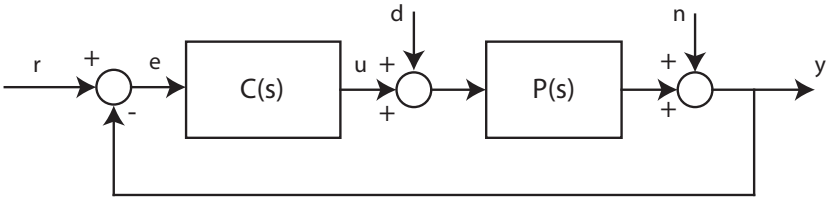


**Figure 2-1:** General feedback system overview

The ability to track a reference signal, reject disturbances or to what degree the system is affected by noise can be captured by four transfer functions. These four transfer functions are called "The gang of four" and are described in [8]. In this thesis, we focus only on the sensitivity function (which captures the effect of noise rejection) and the complementary sensitivity function (which captures the ability to track a signal).

| | | |
|---|---|---|
| Sensitivity function | $\mathrm{S(s)} = \frac{Y(s)}{N(s)}$ | $\frac{1}{1+C(s)P(s)}$ |
| Complementary sensitivity function | $\mathrm{T(s)} = \frac{Y(s)}{R(s)}$ | $\frac{C(s)P(s)}{1+C(s)P(s)}$ |

## 2-2 Sensitivity and complementary sensitivity relationship

The sensitivity function and the complementary sensitivity function are related through Eq. (2-1). It is seen that both functions can not be close to one at the same time. At each frequency the properties of tracking performance and noise rejection must be traded off. If the peak of the complementary sensitivity function needs to be decreased, the sensitivity function will increase for that same peak frequency [13].

$$S(j\omega) + T(j\omega) = \frac{1}{1 + C(j\omega)P(j\omega)} + \frac{C(j\omega)P(j\omega)}{1 + C(j\omega)P(j\omega)} = 1 \tag{2-1}$$

Performance criteria can be determined from the sensitivity and complementary sensitivity function. The complementary sensitivity function $T(j\omega)$ determines the ability to track a reference signal. Reference signals often consists of low frequencies, so for low frequencies, $T(j\omega)$ should have a high magnitude. The sensitivity function $S(j\omega)$ determines the ability to reject measurement noise. Noise often consists of high frequencies, so for great measurement noise rejection, the sensitivity function needs to have a high magnitude for high frequencies. To sum this up:

| | | |
|---|---|---|
| for low frequencies | $T(j\omega) = 1$ | $S(j\omega) = 0$ |
| for high frequencies | $S(j\omega) = 1$ | $T(j\omega) = 0$ |

## 2-3 Loop shaping

When designing feedback controllers, loop shaping is used. It is the industry standard for designing linear controllers and filters. Many company's like Hittech, ASML and others are using this technique. Loop shaping is shaping the open loop bode plot to certain frequency characteristics, such that closed loop specifications will be met. Many closed loop specifications can be translated to open loop frequency domain characteristics for second order systems. With loop shaping, the open loop $L(j\omega)$ is considered, which is defined as $L(j\omega) = C(j\omega)P(j\omega)$. $L(j\omega)$ can be substituted in the sensitivity and complementary sensitivity function:

$$S(j\omega) = \frac{1}{1 + L(j\omega)} \qquad T(j\omega) = \frac{L(j\omega)}{1 + L(j\omega)} \tag{2-2}$$

As said before, tracking performance is determined by a high magnitude of $T(j\omega)$ for low frequencies. This implies a high open loop gain $L(j\omega)$. For no steady state error, infinite gain

is required at 0 rad/s. To achieve this, an integrator is needed in the system. Even if the plant itself has an integrator, integral control is still desired, such that the low frequencies have a high as possible magnitude, to ensure even better tracking.

High frequency noise rejection is necessary as well, to ensure precision. To achieve this, a high magnitude for $S(j\omega)$ is required at high frequencies. This implies a low open loop gain at high frequencies.

From the open loop bode plot, the bandwidth, the phase margin and gain margin can be derived, as can be seen in Figure 2-2. The bandwidth ($\omega_b$) of a system is defined up to which frequency a system can track its input well enough. This is the frequency at which the gain plot crosses the 0 dB line. Phase margin (PM) is defined as how much additional phase lag could be introduced in the open loop to make the closed loop system unstable. This is defined as 180° plus the phase of the open loop system at the bandwidth frequency. The phase margin should be at least positive to guarantee closed loop stability. The gain margin (GM) is defined as how much change in open loop gain is required to make the closed loop system unstable. This is the gain corresponding to the frequency where the phase is $-180°$.

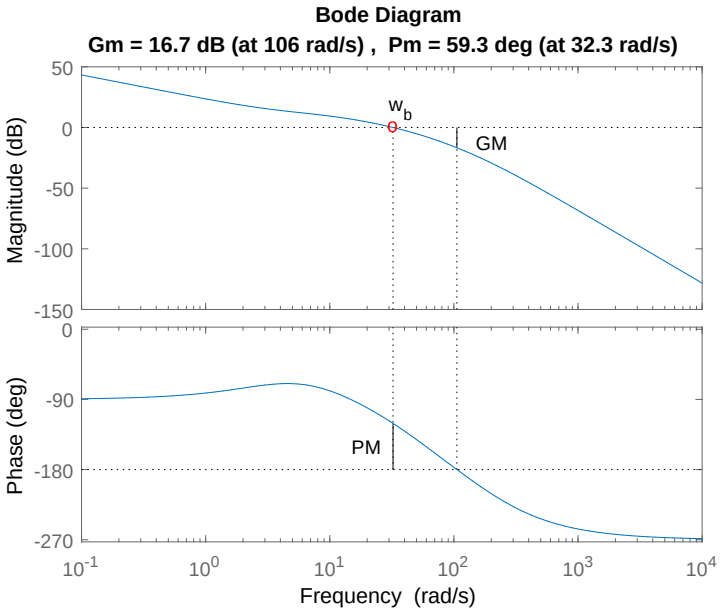


**Figure 2-2:** Bandwidth, phase and gain margin of a system

In Figure 2-2 it is seen that for low frequencies the open loop gain is high (to ensure good tracking) and for high frequencies the open loop gain is low (to ensure good noise rejection).

## 2-4 Limitations of linear control

Linear control has fundamental limitations. Because of this, certain specifications on rise time, overshoot and disturbance rejection e.g. can not be achieved at the same time. In this section, two fundamental limitations of linear control are discussed.

### 2-4-1 Bode's phase gain relation

It is desired to have much phase margin around the bandwidth frequency, since this will add robustness to the system. However, if phase is added around a certain frequency, the open loop slope gain will increase as well. This happens because the magnitude and phase curve are related (in minimum phase systems) through Bode's limitation [8], which is shown in Eq. (2-3). In Eq. (2-3), $n$ represents the slope in the magnitude curve. A slope of -1 means that the magnitude curve drops 20 dB per frequency decade.

$$\angle G(j\omega) = n\ 90^\circ \tag{2-3}$$

When the slope around the bandwidth frequency is increased, the magnitude drops at lower frequencies, and increases at higher frequencies. This will cause poorer reference tracking (less magnitude at low frequencies) and higher noise amplification (higher magnitude at high frequencies). So if phase is added to the system, the slope will increase, causing poorer reference tracking and poorer noise rejection. This can be seen as a trade-off between robustness and performance.

Consider a plant P(s) and controller C(s), which are defined in Eq. (2-4). The open loop Bode plot is shown in Figure 2-3. The plant $P(s)$ is a single mass, which has zero phase margin. When some phase is added by means of a lead controller $C(s)$, performance worses. The tracking performance becomes poorer because in this region the magnitude line drops, and the noise rejection becomes poorer, because the magnitude line increases in this region.

$$P(s) = \frac{1}{s^2}, \qquad C(s) = \omega_p \frac{s + \omega_z}{s + \omega_p} \tag{2-4}$$

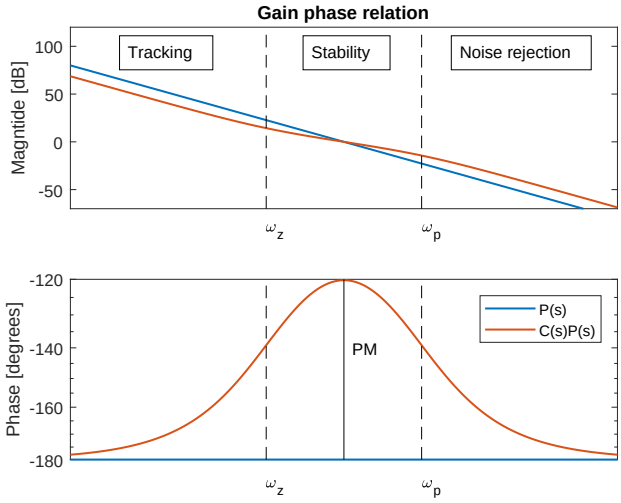


**Figure 2-3:** Trade-off between robustness and performance

### 2-4-2 Waterbed effect

Noise transfer in a system is described by the sensitivity function. In [8] it is shown that for the sensitivity function, Bode's integral formula holds Eq. (2-5). Note that $p_k$ are the poles in the right half plane from the open loop transfer function $L(j\omega)$.

$$\int_0^\infty \ln|S(j\omega)|d\omega = \pi \sum p_k \tag{2-5}$$

When the open loop transfer function has no poles in the right half plane, the integral simplifies to:

$$\int_0^\infty \ln|S(j\omega)|d\omega = 0 \tag{2-6}$$

From Eq. (2-6) it can be seen that the area from the sensitivity function underneath the 0 dB line should be the same as above the 0 dB line. This implies that if for one frequency the sensitivity function is lowered, it has to increase for another frequency. Because of this, it is impossible to have good noise rejection for all frequencies. This effect is called the waterbed effect.

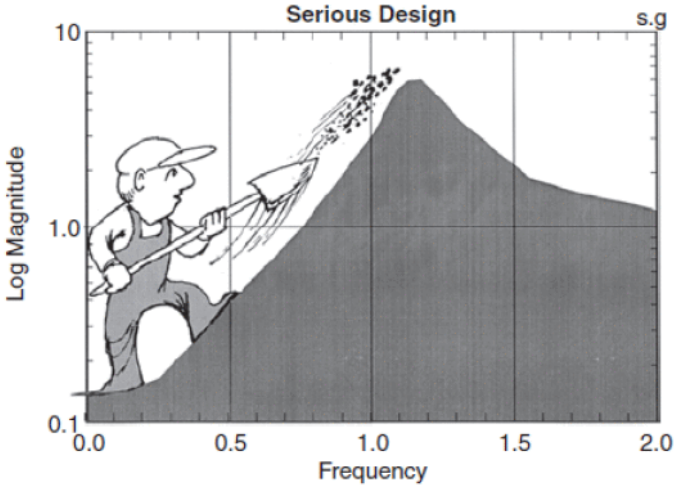


**Figure 2-4:** Illustrated waterbed effect. Image by [1]

## 2-5 Summary

It was seen that linear controllers have fundamental limitations. When phase is added to the system, performance worses. It is desired to add phase to the system, while keeping the same performance. Instead of adding phase to the system, less phase can be subtracted as well to achieve the same. Integrators subtract phase from the system. In the next chapter a non linear integrator is introduced, which shows better performance in the time domain.

# Chapter 3

# Reset systems

In industry, 90% of control is PID, because it has a simple structure and is easily implemented [4]. PID control is linear, and therefore has fundamental limitations, as discussed in the previous chapter. To overcome these limitations, other types of controllers have to be used. The industry does not want to switch to more advanced controllers (like state feedback control, fuzzy state etc) because this often requires a good model of the plant, or requires a lot of computation power. Therefore, PID control needs to be improved. This can be done by introducing non linear behavior. There are several methods to implement non linear behavior, like variable gain [5], split path non linear (SPAN) filters [6], or reset control [9]. In this thesis, reset control is considered. Reset control can improve the integrator behavior by reducing its phase lag by 52°. This can result in less overshoot and faster settling time. However, it can introduce limit cycles in the system, because reset systems can behave differently in steady state than linear systems.

In this chapter, an overview of reset systems is given, such that the reader is familiar with the topic. More detail about the reduced phase lag is given in the next chapter.

## 3-1 Clegg integrator

The Clegg integrator is the main component of a reset system. It can reset its state when the input is zero. The behavior of the Clegg integrator is compared to a linear integrator by means of a sinusoidal input in Figure 3-1. In this example, the Clegg integrator resets its state when the input is zero.

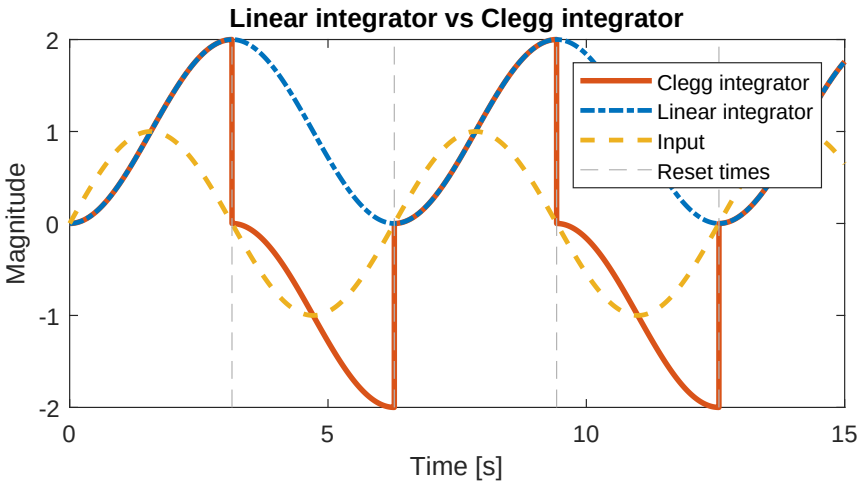


**Figure 3-1:** Linear integrator compared to Clegg integrator with sinusoidal input

The Clegg integrator is noted with an arrow through its state, representing the reset action, as seen in Figure 3-2.

$$\frac{1}{s}$$

**Figure 3-2:** Transfer function representation of Clegg integrator

## 3-2 Introduction in reset systems

A reset system can reset some parameter in the system. The resetting action occurs when a certain condition holds, which is called the reset law. In most cases, the states of the reset system are reset. Resetting a state is done by using a Clegg integrator instead of a linear integrator. Note that an integrator is used in every system which has states, as seen in Figure 3-3. An integrator is not only used for the integral term of a PID controller. Many other examples can be found where integrators are used, like in a low pass filter. With the Clegg integrator, a low pass filter can be reset as well.

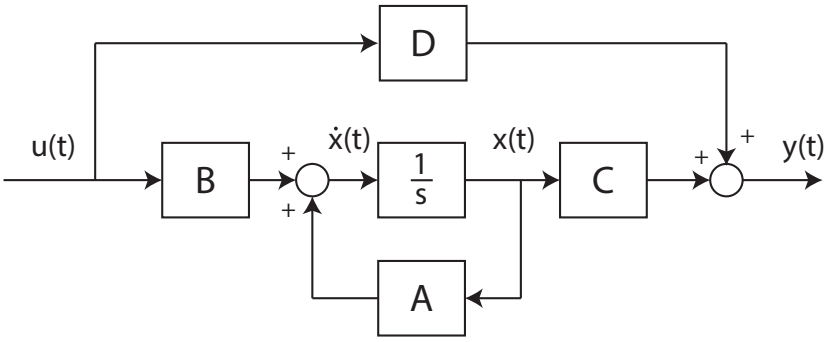


**Figure 3-3:** Linear system in state space form

A state space representation of a general reset system is given in Eq. (3-1). The reset matrix $A_r$ defines to what extent reset occurs (partial reset). When $A_r = 0$, full reset occurs and when $A_r = 1$, no reset occurs and the system behaves like a linear integrator. The time $t^+$ is the time shortly after when the reset occurs.

$$\begin{aligned} \dot{x}(t) &= Ax(t) + Bu(t) & u(t) \neq 0 \\ x(t^+) &= A_r x(t) & u(t) = 0 \\ y(t) &= Cx(t) + Du(t) \end{aligned} \tag{3-1}$$

Consider a reset system consisting only of a Clegg integrator. When the reset system has full reset ($A_r = 0$), the simplified state space model is given by Eq. (3-2).

$$\begin{aligned} \dot{y}(t) &= u(t) & u(t) \neq 0 \\ y(t^+) &= 0 & u(t) = 0 \end{aligned} \tag{3-2}$$

A more common reset system is the first order reset element (FORE). This element can e.g. represent a first order low pass filter with reset. The FORE is shown in Figure 3-4.

$$FORE(s) = \frac{1}{s + a} \tag{3-3}$$

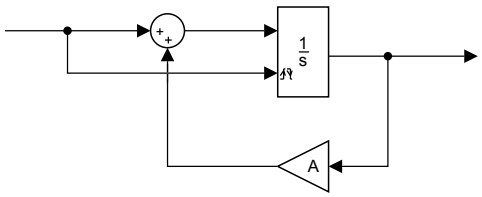


**Figure 3-4:** Overview of a FORE implemented in Simulink

The FORE can be extended to a second order reset element (SORE) or higher orders.

### 3-2-1 Performance of reset systems

When using a reset controller instead of a linear controller, less overshoot can be achieved. Consider a plant $P(s)$, controlled by a first order linear controller $C(s)$ and by a FORE $R(s)$, as in Eq. (3-4). The FORE will reset to zero when its input (the system error $e$) will be zero. It is seen that the FORE has the same controller structure as the linear controller, but the integrator is replaced with a Clegg integrator to achieve reset. In Figure 3-5, the closed loop step responses are plotted for the linear and the reset controller.

$$P(s) = \frac{s+1}{s^2 + 0.2s}, \quad C(s) = \frac{1}{s+1}, \quad R(s) = \frac{1}{s + 1} \tag{3-4}$$

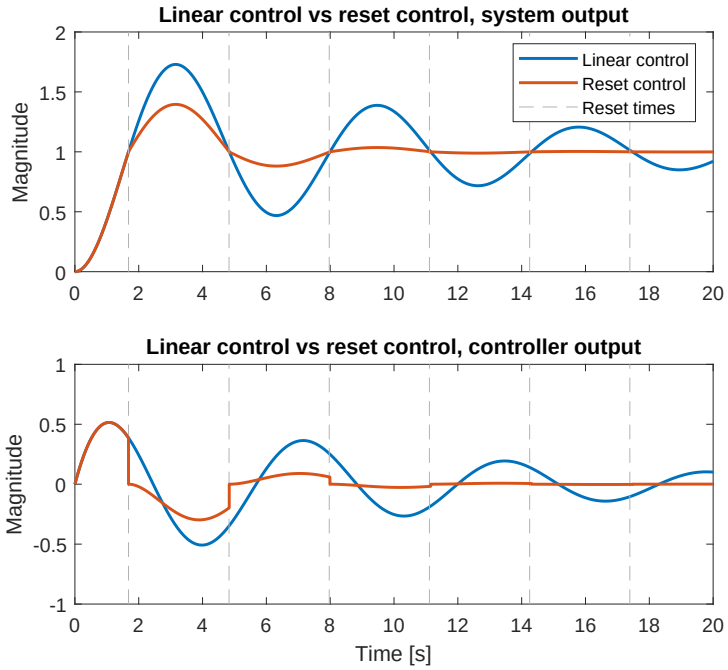


**Figure 3-5:** Step response of linear controller compared to reset controller

It is seen in Figure 3-5 that the reset controller has less overshoot and a faster settling time. When the error of the system is 0 (for example around 1.6 sec), it is seen that the output of the linear controller is still positive, creating overshoot. This happens because the controller itself has some 'inertia', which is caused by the integrator term. The reset controller will reset its controller output to 0, such that the 'inertia' is removed, creating less overshoot. The reset controller keeps resetting every time the system error goes trough zero. Around 14.2 seconds, the system output seems to be 1, but the oscillation is still present, although small.

Reset control is unfortunately not always better then linear control. Consider the next example; a first order plant P(s) is controlled by a PI controller C(s), as seen in Eq. (3-5). A reset controller R(s) is created, which has the same structure as the linear controller, but with a Clegg integrator. As seen in Figure 3-6, the reset controller does go to its reference value, but immediately drops when it hits the reference value, creating oscillations. These oscillations are limit cycles [2].

$$P(s) = \frac{1}{s+0.5}, \quad C(s) = \frac{s+1}{s}, \quad R(s) = \frac{s+1}{\not{s}} \tag{3-5}$$

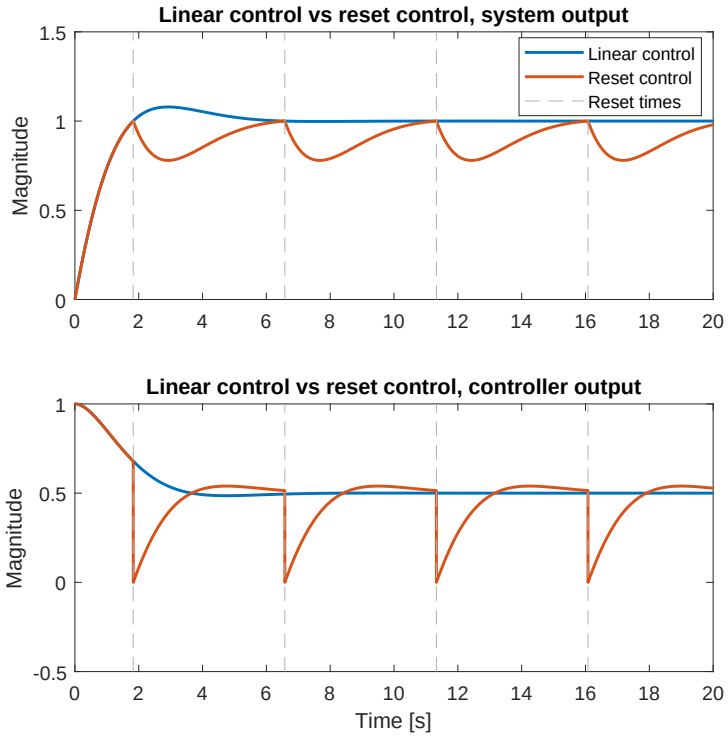


**Figure 3-6:** Step response showing limit cycles using a reset controller

Limit cycles occur in plants where integrator action is needed to drive the plant to the desired output. In other words, limit cycles occur if the plant has a steady state error. A linear integrator, will 'store' energy in its state to maintain zero steady state error. A Clegg integrator will 'remove' this energy, because of the reset action. Because this energy gets removed, the output will suddenly drop. When this happens, limit cycles will occur, and the system undershoots every time the output reaches the reference value. Limit cycles can be removed with adaptive feed forward control [14].

## 3-3 Reset configurations

### 3-3-1 Partial reset

When varying the reset matrix $A_r$ between 0 and 1, partial reset can be achieved. Partial reset resets the states to a fraction of the states. Full reset happens when $A_r = 0$, and no reset happens when $A_r = 1$, like the linear case. For SORE and higher order reset elements, this matrix is usually chosen as $A_r = \gamma I$, where $\gamma$ is the amount of reset.

In the example below, the same systems from the previous sections are simulated. In Figure 3-7a the system from Eq. (3-4) is simulated. In Figure 3-7b the system from Eq. (3-5) is simulated. The partial reset value $\gamma$ is varied from 0 to 1 with steps of 0.2.

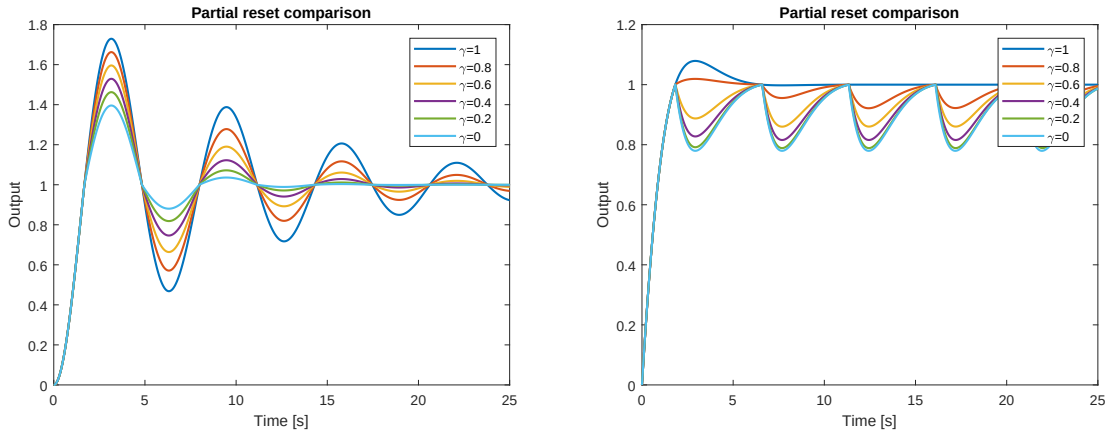


**(a)** System response with partial reset controller showing different levels of overshoot

**(b)** System response with partial reset controller showing limit cycles

**Figure 3-7:** Partial reset comparison

As can be seen from Figure 3-7a, partial reset gives a trade-off between linear and non linear control. In Figure 3-7b, limit cycles still exist, so partial reset does not solve limit cycles in this case. The amount of partial reset does however determine the amplitude of the limit cycle. For some partial reset value between 0.6 and 0.8, the first peak flips sign, such that only undershoot is present in the system.

### 3-3-2 Reset law

In the examples discussed so far, reset occurred when the input of the reset element was zero. Other reset laws are possible as well, like resetting within a certain reset band or resetting at a fixed time interval. These two reset laws are discussed in this section.

#### Reset band

Instead of resetting the integrator when the input is zero, it resets when the input enters a certain band. This band is usually chosen to lie around zero with a certain range $\delta$. A reset band may provide phase lead in time delay systems [2]. A reset band is mathematically described in Eq. (3-6). In Eq. (3-6), the band has a fixed width, but the band could be of variable width as well [12].

$$\begin{aligned} \dot{x}(t) &= Ax(t) + Bu(t) && u(t), \dot{u}(t) \notin B_\delta \\ x(t^+) &= A_r x(t) && u(t), \dot{u}(t) \in B_\delta \\ y(t) &= Cx(t) + Du(t) \end{aligned} \tag{3-6}$$

$$\text{with } B_\delta = (x, y) \in R^2 | (x = -\delta \wedge y > 0) \vee (x = \delta \wedge y < 0)$$

### Fixed time reset control

In [15], Zheng et al proposed a new reset law where reset occurs at fixed time instances. In [16], Gup et al used this design technique in hard disk drive systems. Fixed time reset control is defined in Eq. (3-7).

$$\begin{aligned} \dot{x}(t) &= Ax(t) + Be(t) & t \neq t_k \\ x(t^+) &= A_r x(t) & t = t_k \\ u(t) &= Cx(t) + De(t) \end{aligned} \tag{3-7}$$

In [15], it is seen that the after reset value needs to be optimized to exclude limit cycles. When model uncertainties are present, this could influence the performance of the system.

## 3-3-3 PI+CL control

In Figure 3-6 it was seen that the Clegg integrator didn't show overshoot, but did show limit cycles. To get a combination of less overshoot and no steady state error, a combination of a linear controller and a reset controller can be implemented. This is often named a PI+CI controller. In this controller, the PI controller is called the base system and the CI controller the reset system. Varying the contribution of both controllers with a factor $p_{reset}$, the amount of non linearity can be chosen. When $p_{reset} = 1$, the integral part is a Clegg integrator, and when $p_{reset} = 0$, the integral part is a linear integrator. The PI+CL controller structure is given in Eq. (3-8) and a system overview is given in Figure 3-8. In [2] the PI+CL is explained more, and in [17] some design rules are given.

$$PI + CL = k_p \left(1 + \frac{1}{\tau_i}\left(\frac{1 - p_{reset}}{s} + \frac{p_{reset}}{s}\right)\right) \tag{3-8}$$

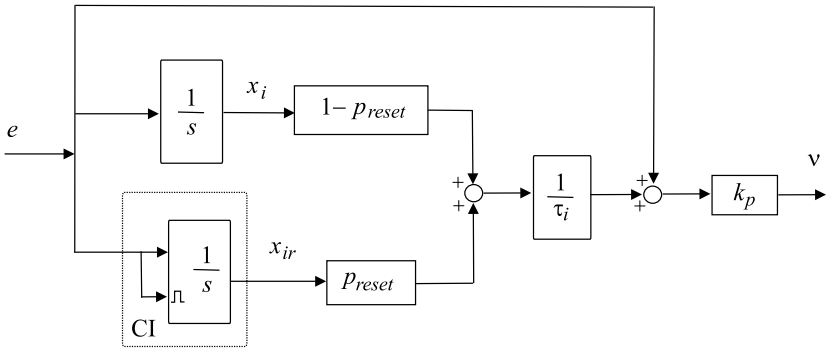


**Figure 3-8:** Overview of PI+CL controller. Image by [2]

In Figure 3-9 the performance increase can be seen for implementing a PI+CL controller. The system is the same system as in Eq. (3-5), but now the PI+CL controller is implemented, as shown in Figure 3-8. The parameter $p_{reset}$ is tuned to 0.2, $\tau_i = 1$ and $k_p = 1$. It can be seen that the limit cycle disappears, the overshoot becomes less and that the settling time decreases.

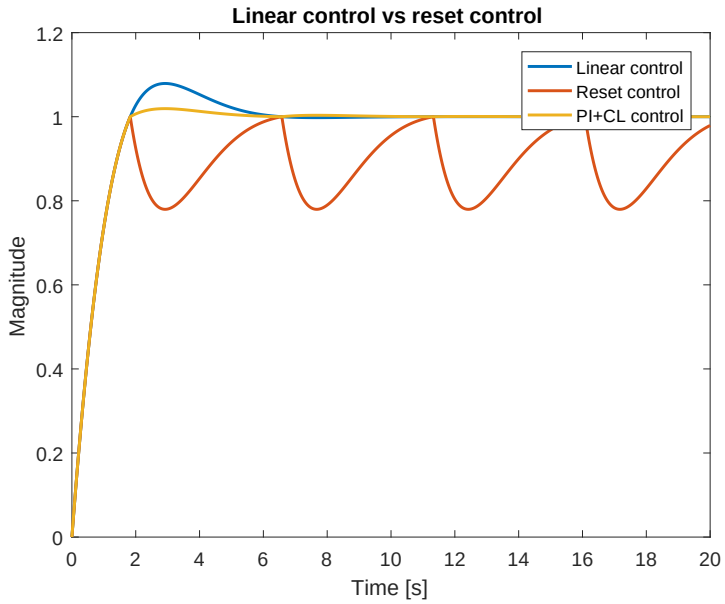


**Figure 3-9:** System response of PI+CL controller compared to linear and reset controller

## 3-4 Stability analysis

There are many methods to prove stability for reset systems. Most stability conditions require the equivalent linear system to be stable [2, 18, 19]. We are however interested in marginal stable reset systems (this will be explained in the next chapter), which do not have stable linear equivalents. The requirement to have a linear equivalent stable system it thus too conservative. The most advanced result paper is found which proves the (in)stability of a reset system subjected to zero inputs [20]. This paper is used to prove (in)stability of reset systems in this thesis. The paper considers zero input systems, but the method can be used for step inputs as well, since step inputs can be rewritten as a zero input with an extra feedforward term, as seen in Figure 3-10. In this section, the method from [20] is explained.

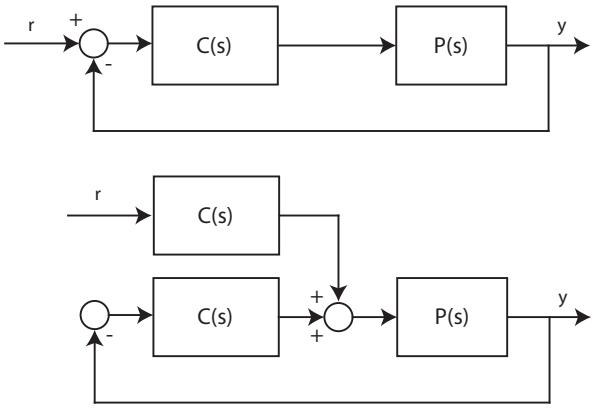


**Figure 3-10:** Step input represented as zero input with feed forward

The stability criterion states that the time interval $\tau$ between reset instances has to be known. When the reset interval is known, stability can be proven. Assume a second order plant without feed trough matrix $D$, so $G(s) = C(sI - A)^{-1}B$. When this plant is controlled by a Clegg integrator and subjected to zero input, the state space system from Eq. (3-9) is formed. In here, $x_c$ is the state of the controller and $x_p$ the state of the plant.

$$\begin{aligned} \dot{x}_p(t) &= Ax_p(t) + Bx_c(t) \\ \dot{x}_c(t) &= -y(t) && y(t) \neq 0 \\ x_c(t) &= 0 && y(t) = 0 \\ y(t) &= Cx_p(t) \end{aligned} \tag{3-9}$$

The zero crossing times of $y(t)$ are collected in the ordered set $(t_i \leq t_{i+1},\ i = 1, 2, ...,)$. Between the crossing times of the reset action, the plant states behaves like an LTI system.

$$x(t) = P(t - t_i)x(t_i) \tag{3-10}$$

Of which

$$P(t) = \begin{bmatrix} I & 0 \end{bmatrix} e^{\bar{A}t} \begin{bmatrix} I \\ 0 \end{bmatrix} \qquad \text{with} \qquad \bar{A}(t) = \begin{bmatrix} A & B \\ -C & 0 \end{bmatrix} \tag{3-11}$$

The reset interval $\tau$ can be obtained if the smallest positive $\tau$ is found, for which $C$ is an eigenvector of $P(\tau)$ [20]. This is hard to calculate analytically, and therefore another approach is used; A reset system is simulated in Simulink with high tolerances. This reset system can e.g. be a Clegg integrator controlling a second order plant. A step input is applied to the closed loop system. The system will start oscillating, and the crossing times are stored, such that the reset interval $\tau$ can be calculated. When the reset interval is known, the $P$ matrix can be calculated, of which the eigenvalues are checked. When the biggest eigenvalue is smaller than 1, the system is stable. When the biggest eigenvalue is exactly 1, the system is marginally stable. When the biggest eigenvalue is larger than 1, the system is unstable.

# Chapter 4

# Frequency analysis of reset systems

For linear systems, frequency analysis and loop shaping are a common way to analyze and design controllers. For reset systems to be a useful tool in industry, these frequency domain methods should be applicable as well. In this chapter, we address how we can approximate frequency responses with describing functions, and show what the limitations of that approach are.

## 4-1 Describing functions

For linear systems, transfer functions can be used to analyze the system in the frequency domain. For non linear systems, transfer functions do not exist, since they only represent linear systems. Non linear elements can also depend on parameters other than frequency, like amplitude. To overcome this problem, describing functions are often used to describe a non linear system in the frequency domain.

A describing function approaches a transfer function for non linear elements. It is the linear approximation of the steady state output considering only the first harmonic of the output [21]. Examples of how to use the describing function can be found in [22, 23].

There are several types of describing functions [24]. In this thesis the sinusoidal input describing function (SIDF) is considered, since this represents a transfer function the most. It is defined as the phasor representation of the output divided by the phasor representation of the input at a certain frequency [25]. This is similar to what a transfer function does. The describing function can be created by applying a sinusoidal input and calculating its time domain response. When this response is Fourier transformed, a Fourier series is created. The describing function considers only the first harmonic of the Fourier series.

The Clegg integrator does not depend on its input amplitude (like other non linear elements), but only on its input frequency. Because of this, it is much easier to represent the describing function of a reset system in the same way as a transfer function. In [10], the describing function for a reset system with the same structure are Eq. (3-1) is given. This is shown in Eq. (4-1).

$$
\begin{aligned}
G(\omega) &= C(j\omega I - A)^{-1}(I + j\Theta_D(\omega))B + D \\
\text{with } \Theta_D(\omega) &= -\frac{2\omega^2}{\pi}\Delta(\omega)[\Gamma_r(\omega) - \Lambda^{-1}(\omega)] \\
\Lambda(\omega) &= \omega^2 I + A^2 \\
\Delta(\omega) &= I + e^{\frac{\pi}{\omega}A} \\
\Delta_r(\omega) &= I + A_r e^{\frac{\pi}{\omega}A} \\
\Gamma_r(\omega) &= \Delta_r^{-1}(\omega)A_r\Delta(\omega)\Lambda^{-1}(\omega)
\end{aligned}
\tag{4-1}
$$

### 4-1-1 Describing function of the Clegg integrator

The describing function of the Clegg integrator (Eq. (4-2)) is obtained if the following system matrices are plugged in Eq. (4-1) : $A = 0,\ B = 1,\ C = 1,\ D = 0,\ A_r = 0$. Notice that there are two notations, which both are used in literature.

$$
\begin{aligned}
CI(\omega) &= \frac{1}{j\omega}\left(1 + j\frac{4}{\pi}\right) \\
&= \frac{1}{j\omega}1.62e^{j52^\circ}
\end{aligned}
\tag{4-2}
$$

From now on, when we talk about the frequency response of the Clegg integrator, we consider its first order describing function. From Eq. (4-2) it can be seen that the Clegg integrator has a higher magnitude response, but also a phase lead of 52° compared to the linear integrator. It is this last characteristic that make reset systems so interesting. The Clegg integrator has the same frequency behavior as a linear integrator, but with only 38° phase lag, instead of 90°. A frequency domain comparison is shown in Figure 4-1 between the linear and Clegg integrator.

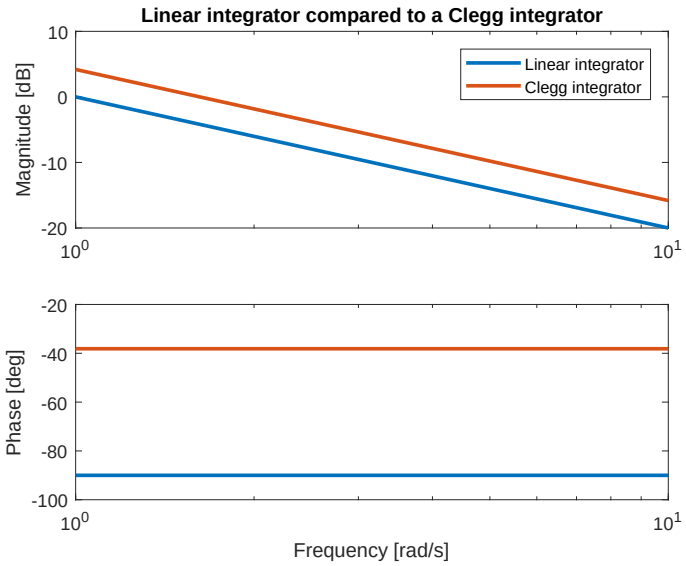


**Figure 4-1:** Frequency response comparison of a linear integrator and a Clegg integrator

## 4-2 Describing function error

As said before, the describing function describes only the first harmonic of its output. The output of a Clegg integrator contains jumps, resulting in sharp edges. These sharp edges cannot accurately be captured with a single sine wave, which the first order describing function tries to do. This is easily seen by performing the following experiment. A Clegg integrator is simulated, by applying an input $u(t) = sin(2t)$. When looking at the describing function of the Clegg integrator, the describing function suggests that the output should be a sine wave with an amplitude of 0.81 and a phase shift of -38°. However, the output looks a lot different, as can be seen in Figure 4-2. There is a big difference between the output of the Clegg integrator and the output the describing function approximates.

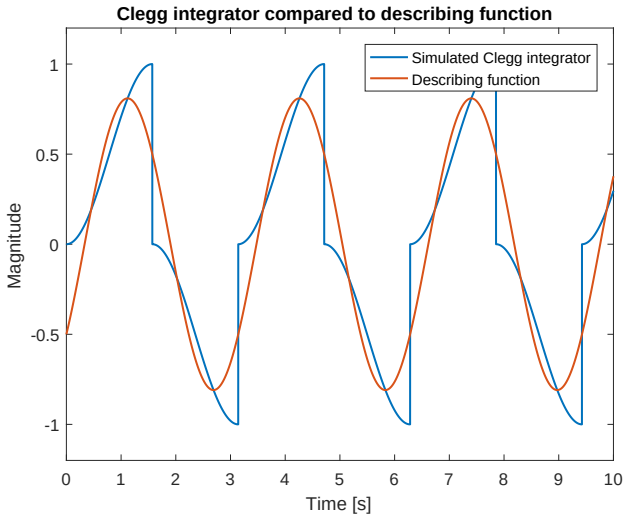


**Figure 4-2:** Simulation of real output compared to describing function for the Clegg integrator

## 4-3 Loop Shaping

In linear feedback control, controllers can be designed in the frequency domain using loop shaping. When looking at the open loop transfer function of the system, stability is guaranteed as long as the system has a open loop positive phase margin, as described in Section 2-3. In this section, the possibility of loop shaping with reset systems is investigated.

Consider a feedback system with plant $P(s)$ and reset controller $R(s)$, as in Eq. (4-3). To get the frequency response of the plant and the controller, a conversion from the Laplace notation to the frequency notation has to be made. When the two frequency functions are multiplied with each other, the open loop frequency response is known, which is shown in Figure 4-3.

$$\begin{aligned} R(s) &= \frac{1}{\cancel{s}} & P(s) &= 0.15\frac{s+2}{s^2+0.2s} \\ R(\omega) &= \frac{1}{j\omega}(1+j\frac{4}{\pi}) & P(j\omega) &= 0.15\frac{j\omega+2}{(j\omega)^2+0.2j\omega} \end{aligned} \tag{4-3}$$

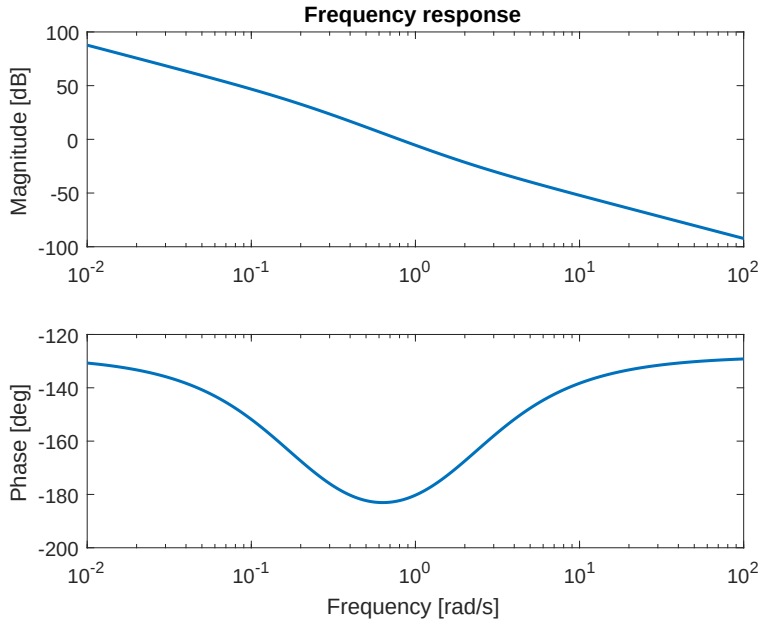


**Figure 4-3:** Unstable open loop frequency response of system controlled by a Clegg integrator

In Figure 4-3, the open loop is calculated for 10000 frequencies between $10^{-2}$ rad/s and $10^{2}$ rad/s. The crossover frequency is calculated with interpolation. With the crossover frequency, the phase of the open loop system is calculated, and thus the phase margin is known. The phase margin for this system is -2.33°, so it is expected to behave unstable when closing the loop. However, the output is stable, as seen in Figure 4-4.

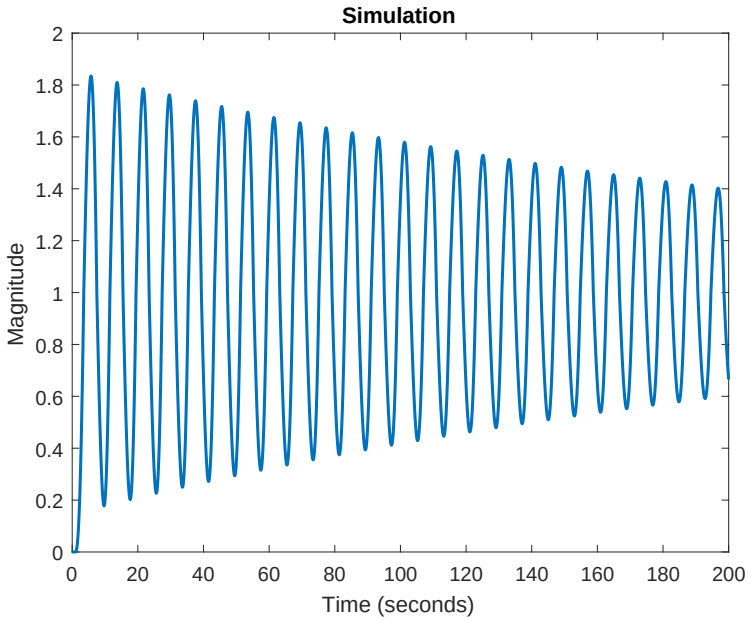


**Figure 4-4:** Stable closed loop step response for unstable describing function

When applying the stability criterion from Section 3-4, eigenvalues of 0.854 (2x) are obtained. Because the eigenvalues are smaller than 1, stability is proven.

It is concluded that the describing function produces inaccurate results to do loop shaping with this plant. In the next section it is explored if the same inaccuracy is seen for other plants.

### 4-3-1 Accuracy of the describing function

The plant from the previous section was chosen to explain the error of the describing function. One could see this plant as an integrator with a lead filter, but these plants are not very common in industry. More common plants are second order systems like mass damper systems or mass spring damper (MSD) systems. In this section, it is investigated for these type of plants how accurate the describing function is.

Mass damper and MSD systems have a phase response which goes to -180°. When controlling such a system with a Clegg integrator, the phase will pass -180° at some point, and will go to -218°. For both systems, there exists a control gain for the Clegg integrator such that the closed loop performance is marginally stable. Marginal stability is important, because this can be tested in the time domain and in the frequency domain. With the stability condition proposed in Section 3-4, marginal stability can be tested in the time domain. When the frequency response is known, marginal stability can also be tested in the frequency domain. The frequency response is made by the describing function from the Clegg integrator. This is an approximation, so the frequency response is expected not to be exact. If the system is tuned to perform marginally stable in the time domain, the accuracy of the describing function can be verified.

In the next two parts the accuracy of the first order describing function is tested for mass damper systems and for mass spring damper (MSD) systems. Both the systems will be controlled by a Clegg integrator with a gain $K$. A step input will applied to the closed loop system. The gain $K$ will be fine tuned by hand to find the point of marginal stability. This point is checked with the stability condition from Section 3-4. It is practical impossible to tune the system to perform exactly marginally stable, so it is tuned such that the system is slightly stable. It is decided that when the biggest eigenvalue is between 0.999 and 1, the system is marginally stable. Next, the crossover frequency is found by interpolating the results from the frequency response. With the crossover frequency, the corresponding phase is calculated. Because the system is tuned to perform marginally stable, the phase should be exactly -180° at the crossover frequency.

#### Mass damper systems

Consider a mass damper system $P(s)$ controlled by a Clegg integrator $R(s)$ with gain $K$, as in Eq. (4-4). Mass damper systems start at -90° and go to -180°. When controlling this with a Clegg integrator, the phase of the open loop system will pass -180° and go to -218°.

$$R(s) = K\,\frac{1}{\cancel{s}} \qquad P(s) = \frac{1}{s^2 + as} \tag{4-4}$$

A few mass damper systems are simulated by varying the value $a$. The gain $K$ is increased until the system performs marginally stable. This gain $K$ is fine tuned by hand, and checked with the stability criterion. In Table 4-1 the results are listed for several values of $a$. The gain $K$ is listed, and the corresponding phase at the crossover frequency. Because the systems perform marginally stable, the phase at the crossover frequencies should be exactly -180°.

It is seen that the phases of all the systems are equally off by 0.69°. It it seen that for every increase in value of $a$, the gain $K$ can be cubicly increased to find a marginally stable system. Three systems with different values for $a$ are plotted in Figure 4-5, with corresponding values of K to make the system marginally stable. It is concluded that the first order describing function is evenly inaccurate for any mass damper system.

**Table 4-1:** Values for marginally stable mass damper systems controlled by a Clegg integrator

| $a$ | $K$ | phase (°) |
|---|---|---|
| 0.100 | 0.0017306 | -180.6908 |
| 0.200 | 0.013845 | -180.6910 |
| 0.400 | 0.111 | -180.6910 |
| 0.800 | 0.886 | -180.6912 |
| 1.000 | 1.731 | -180.6908 |
| 10.000 | 1730.600 | -180.6908 |
| 100.000 | 1730670.000 | -180.6913 |

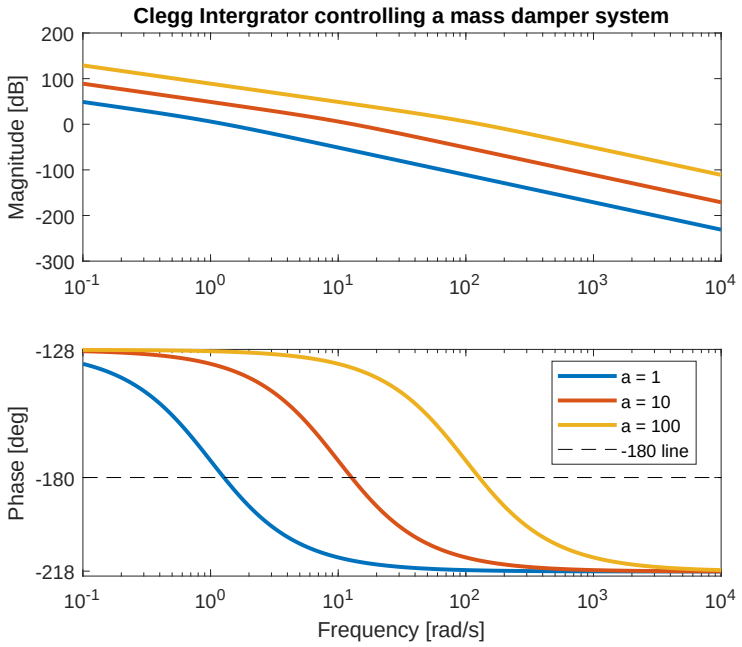


**Figure 4-5:** Frequency response of marginally stable mass damper systems, different values of $a$ with corresponding $K$

### Mass spring damper systems

The procedure for testing mass damper systems is used as well for mass spring damper (MSD) systems. MSD systems have transfer functions as shown in Eq. (4-5). The parameter $\omega_n$ represents the natural frequency of the system and $\zeta$ the amount of damping. These systems go to -218° as well, passing -180°. Because of this, there exists a gain $K$ for the Clegg integrator such that the closed loop system performs marginally stable. We fine tune the gain $K$ by hand, and check for marginally stability using the stability condition from Section 3-4.

$$R(s) = K \frac{1}{s} \qquad P(s) = \frac{\omega_n^2}{s^2 + 2\zeta\omega_n s + \omega_n^2} \tag{4-5}$$

Several MSD systems are created which performs marginally stable. First the natural frequency $\omega_n$ is varied, and later the damping factor $\zeta$. In Table 4-2 the natural frequency $\omega_n$, the damping factor $\zeta$, the gain value $K$ and the phase at the crossover frequency are listed. In Figure 4-6, some MSD systems are simulated with different values for $\omega_n$ and $\zeta$, with corresponding values for $K$ to create a marginally stable system. It is seen that when changing the damping $\zeta$, the gradient of the phase ($\nabla$) changes at the crossover frequency. Because of this, the gradient of phase is listed as well in Table 4-2. The gradient of phase is measured in degrees per decade.

**Table 4-2:** Values for marginally stable mass spring damper systems controlled by a Clegg integrator

| $\omega_n$ | $\zeta$ | $K$ | phase (°) | $\nabla$ phase (°/dec) |
|---|---|---|---|---|
| 1000 | 0.2 | 666.66 | -180.1691 | -258.04 |
| 100 | 0.2 | 66.64 | -180.1631 | -258.04 |
| 10 | 0.2 | 6.664 | -180.1631 | -258.04 |
| 1 | 0.2 | 0.6665 | -180.1654 | -258.04 |
| 10 | 0.0125 | 0.2581 | -180.0024 | -4143.23 |
| 10 | 0.05 | 1.136 | -180.0103 | -1011.23 |
| 10 | 0.2 | 6.66 | -180.1467 | -258.04 |
| 10 | 0.6 | 50.600 | -180.4599 | -104.09 |
| 10 | 1.2 | 283.900 | -180.6064 | -75.71 |
| 10 | 2.4 | 2005.800 | -180.6668 | -66.90 |
| 10 | 4.8 | 15497 | -180.6849 | -64.52 |
| 10 | 9.6 | 122866 | -180.6897 | -63.91 |
| 10 | 19.2 | 980700 | -180.6908 | -63.76 |

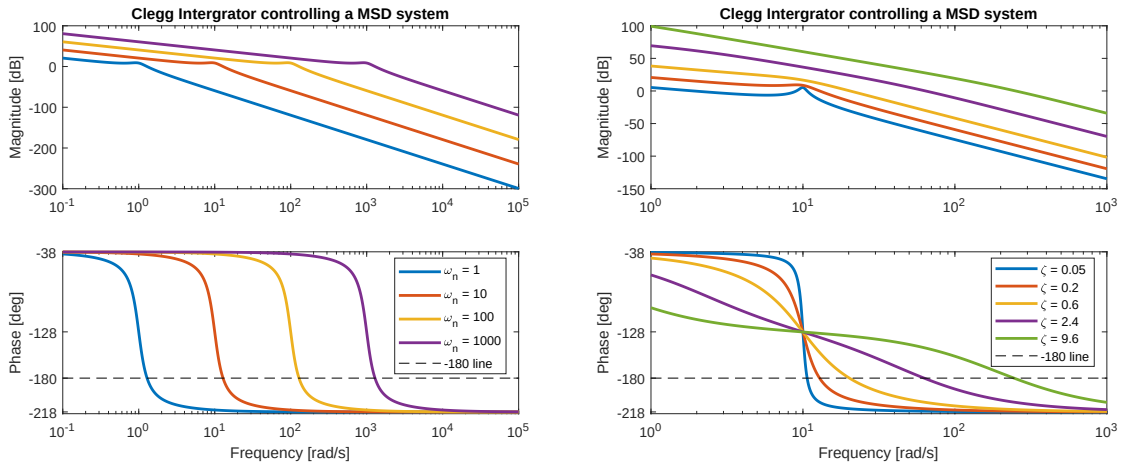


**(a)** MSD system with varying $\omega_n$

**(b)** MSD system with varying $\zeta$

**Figure 4-6:** Frequency response of marginally stable MSD systems, different values of $\omega_n, \zeta$ with corresponding $K$

In Table 4-2 it is seen that when the natural frequency $\omega_n$ is changed, the gain could be increased linearly with the change in natural frequency. The accuracy of the describing function has a constant offset of 0.16°. The gradient of the phase is also constant. When the damping $\zeta$ is altered, the gradient of the phase changes. When the damping is low, the gradient of the phase is high (in absolute value), and the phase of the first order describing function is close to -180°, implying an accurate phase. When the damping is high, the gradient of the phase is low, and phase of the first order describing function drifts away from -180°.

The gradient of phase for a mass damper system is -63.71°/dec. This is almost the same gradient as for a MSD system with a high damping. A MSD system with high damping does act like a mass damper system, so it is expected that the gradient of phase is the same.

It is suspected that the accuracy of the describing function is depended on the gradient of the phase. When the gradient of the phase is largely negative, the describing functions becomes more accurate. When the gradient of phase is small, the describing function becomes more inaccurate. It is noticed that the describing function has an different accuracy for different plants. It is suspected that the accuracy of the describing function is influenced by the plant doing loop shaping.

It is seen that the describing function is inaccurate, but in our favor. The describing function predicts instability for mass damper and MSD systems, but it is seen that the system was still (marginally) stable. This is in our favor, since less phase margin is expected by the describing function than happens in reality.

It was seen in Section 4-2 that the describing function is not accurate in the time domain, and this section also proofs its inaccuracy in the frequency domain. If the describing function is not reliable for stability, then we can not know how accurate it is for tracking, disturbance rejection and noise attenuation. To make the describing function more accurate, higher orders needs to be introduced.

# Chapter 5

# HOSIDF

Loop shaping is extremely useful when designing controllers. As seen in the previous chapter, the relation between phase margin and stability cannot be translated to non linear reset control, because the describing function is not accurate enough. There are papers which describe methods to deal with the inaccuracy of the describing function, like [26], where they discuss the describing function approach for a rate limiter element. It is however more desired to create a reliable method of describing function analysis, than to learn to deal with an inaccurate method. In current describing function analysis, only the first harmonic of a Fourier series is considered. It is desired to extend the describing function to higher orders, making the frequency domain analysis more accurate.

With simulation, the full Fourier series of an output signal from the Clegg integrator can be calculated. With the Fourier series, the amplitude and phase shift for each harmonic can be found. However, calculating the Fourier series takes a lot of time, since individual experiments and time consuming calculations per frequency are needed. Instead of calculating the Fourier series of a simulated output, an analytical solution is found.

Nuij [3] created a framework to analyze higher order describing functions for non linear elements. This framework will be used for the non linear reset elements. Other work which uses this framework can be found in [27, 28].

The Clegg integrator creates a non linear output, which consists of multiple sine waves because of its periodic properties. Because of this, the Clegg integrator can be seen as a virtual harmonic generator, as described by [3], and seen in Figure 5-1. When a sine wave of frequency $\omega$ is inserted, the virtual harmonic generator will create harmonics of frequency $\omega, 2\omega, 3\omega, ..., n\omega$. These harmonics are inserted in several describing functions (denoted with $H_n(\omega)$ in Figure 5-1). The describing functions will transform the harmonics with a certain amplitude and certain phase shift, like a transfer function. These describing functions form together the higher order sinusoidal describing function (HOSIDF). As noted before, the behavior of the Clegg integrator does not depend on its input amplitude, but only on its input frequency. This makes the analysis much easier.

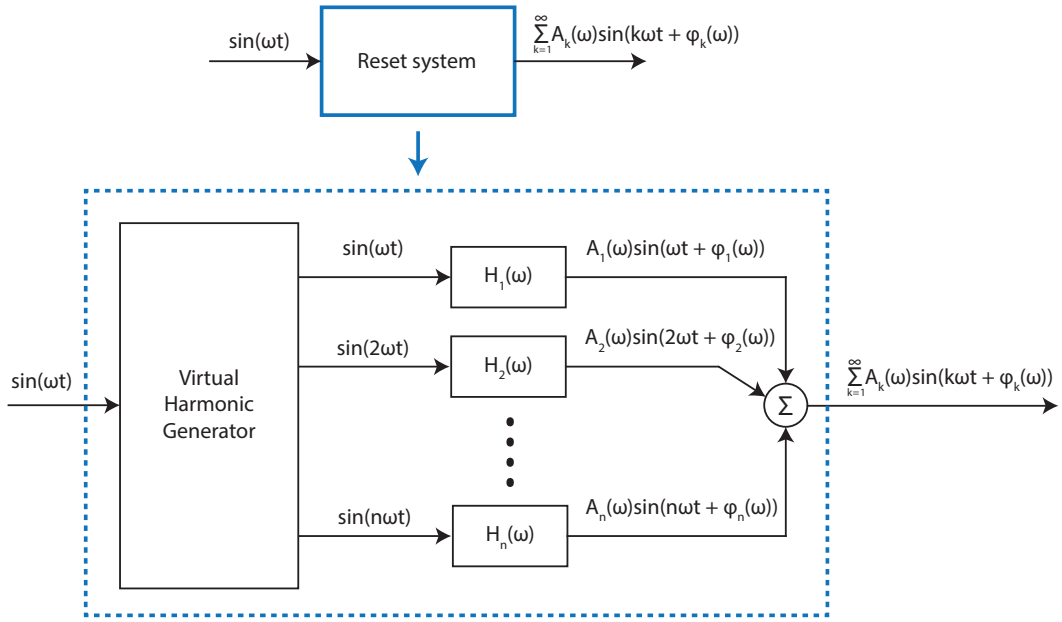


**Figure 5-1:** Block diagram representation of the HOSIDF, image based on [3]

## 5-1 Analytical solution

Guo et al [10] calculated analytically the describing function of the first harmonic for a general reset system. Based on their work, a derivation is calculated for the HOSIDF. Notice that in [10], the reset matrix is defined as $D$. This is confusing since $D$ usually represents the feed through matrix of a state space model. In this thesis, $A_r$ is used to represent the reset matrix.

**Theorem 1.** *For a reset system given in Eq. (5-1), the HOSIDF is calculated by Eq. (5-2).*

$$\begin{aligned} \dot{x}(t) &= Ax(t) + Bu(t) & u(t) &\neq 0 \\ x(t^+) &= A_r x(t) & u(t) &= 0 \\ y(t) &= Cx(t) + Du(t) \end{aligned} \tag{5-1}$$

$$G(\omega, n) = \begin{cases} C(j\omega I - A)^{-1}(I + j\Theta_D(\omega))B + D & \text{for } n = 1 \\ C(j\omega n I - A)^{-1} j\Theta_D(\omega) B & \text{for odd } n \geq 2 \\ 0 & \text{for even } n \geq 2 \end{cases}$$

$$\begin{aligned} \text{with} \quad \Theta_D(\omega) &= -\frac{2\omega^2}{\pi}\Delta(\omega)[\Gamma_r(\omega) - \Lambda^{-1}(\omega)] \\ \Lambda(\omega) &= \omega^2 I + A^2 \\ \Delta(\omega) &= I + e^{\frac{\pi}{\omega}A} \\ \Delta_r(\omega) &= I + A_r e^{\frac{\pi}{\omega}A} \\ \Gamma_r(\omega) &= \Delta_r^{-1}(\omega) A_r \Delta(\omega) \Lambda^{-1}(\omega) \end{aligned} \tag{5-2}$$

*Proof.* This proof is divided in two parts. A reset element can be divided into a linear and non linear part, as seen in Figure 5-2. The $B$ and $C$ matrix are chosen to be in the non linear part for convenience, although they behave linear. First, an analysis for the non linear part is made, and later for the linear part.

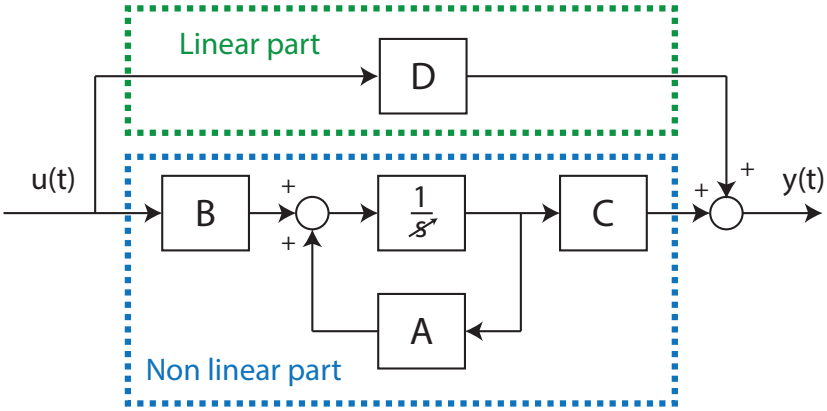


**Figure 5-2:** Non linear and linear part of a reset system

The following notation is defined for convenience:

$$\begin{aligned}\Lambda(\omega) &= \omega^2 I + A^2 \\ \Delta(\omega) &= I + e^{\frac{\pi}{\omega}A} \\ \Delta_r(\omega) &= I + A_r e^{\frac{\pi}{\omega}A} \\ \Gamma_r(\omega) &= \Delta_r^{-1}(\omega) A_r \Delta(\omega) \Lambda^{-1}(\omega)\end{aligned} \tag{5-3}$$

The linear part is analyzed by setting the feed through matrix $D$ in Eq. (5-1) to zero. When a reset element is subjected to a sinusoidal input of $u(t) = sin(\omega t)$, an equation for the steady output $y_{ss}(t)$ can be calculated, as can be found in [10].

$$\begin{aligned}y_{ss}(t) &= Ce^{At}\theta_k(\omega) - C\Lambda^{-1}(\omega)[\omega I cos(\omega t) + A sin(\omega t)]B \\ \theta_k(\omega) &= (-1)^{k+1} e^{-At_k}[\Gamma_r(w) - \Lambda^{-1}(\omega)]\omega B\end{aligned} \tag{5-4}$$

The Fourier series for the first harmonic is already given in [10], so only higher orders will be calculated ($n \geq 2$):

$$\begin{aligned}Y_{ss}(\omega, n) &= \frac{\omega}{2\pi}\int_0^{\frac{2\pi}{\omega}} y_{ss}(t) e^{-j\omega n t} dt \\ &= \frac{\omega C}{2\pi}(I_1 + I_2) - \frac{\omega C \Lambda^{-1}(\omega)}{2\pi}(\omega J_1 + A J_2)B\end{aligned} \tag{5-5}$$

With

$$\begin{aligned}I_1 &= \int_0^{\frac{\pi}{\omega}} e^{At}\theta_0(\omega) e^{-j\omega n t} dt \\ &= \theta_0(\omega)(A - j\omega n I)^{-1}(e^{\frac{\pi}{\omega}A}(-1)^n - 1) \\ &= -[\Gamma_r(\omega) - \Lambda^{-1}(\omega)]\omega B(A - j\omega n I)^{-1}(e^{\frac{\pi}{\omega}A}(-1)^n - 1)\end{aligned}$$

$$
\begin{aligned}
I_2 &= \int_{\frac{\pi}{\omega}}^{\frac{2\pi}{\omega}} e^{At}\theta_1(\omega)e^{-j\omega nt}dt \\
&= \theta_1(\omega)(A - j\omega nI)^{-1}(e^{\frac{2\pi}{\omega}A} - e^{\frac{\pi}{\omega}A}e^{-j\pi n}) \\
&= [\Gamma_r(\omega) - \Lambda^{-1}(\omega)]\omega B(A - j\omega nI)^{-1}(e^{\frac{\pi}{\omega}A} - e^{-j\pi n})
\end{aligned}
$$

$$
\begin{aligned}
J_1 &= \int_{0}^{\frac{\pi}{\omega}} e^{-j\omega nt}cos(\omega t)dt \\
&= 0 \quad \text{for } (n \geq 2)
\end{aligned}
$$

$$
\begin{aligned}
J_2 &= \int_{0}^{\frac{\pi}{\omega}} e^{-j\omega nt}sin(\omega t)dt \\
&= 0 \quad \text{for } (n \geq 2)
\end{aligned}
$$

$$
\begin{aligned}
Y_{ss}(\omega, n) &= \frac{\omega C}{2\pi}(I_1 + I_2) \quad \text{for } (n \geq 2) \\
&= \frac{\omega C}{2\pi}[\Gamma_r(\omega) - \Lambda^{-1}(\omega)]\omega B(A - j\omega nI)^{-1}\big[ - e^{\frac{\pi}{\omega}A}(-1)^n + 1 + e^{\frac{\pi}{\omega}A} - e^{-j\pi n}\big]
\end{aligned}
\tag{5-6}
$$

It is noticed that the last term in Eq. (5-6) becomes 0 for even numbers of $n$. Rewriting Eq. (5-6) with this in mind:

$$
Y_{ss}(\omega, n) = \begin{cases} \frac{\omega^2 C}{\pi}(A - j\omega nI)^{-1}\Delta(\omega)[\Gamma_r(\omega) - \Lambda^{-1}(\omega)]B & \text{for odd n} \geq 2 \\ 0 & \text{for even n} \geq 2 \end{cases} \tag{5-7}
$$

The input signal $u(t)$ stays the same as described in [10], such that the final describing function becomes:

$$
G(\omega, n) = \frac{Y_{ss}(\omega, n)}{U(j\omega)} \qquad \text{with} \quad U(j\omega) = -\frac{j}{2} \tag{5-8}
$$

$$
G(\omega, n) = \begin{cases} C(j\omega I - A)^{-1}(I + j\Theta_D(\omega))B & \text{for } n = 1 \\ C(j\omega nI - A)^{-1}j\Theta_D(\omega)B & \text{for odd } n \geq 2 \\ 0 & \text{for even } n \geq 2 \end{cases} \tag{5-9}
$$

$$
\text{with} \quad \Theta_D(\omega) = -\frac{2\omega^2}{\pi}\Delta(\omega)[\Gamma_r(\omega) - \Lambda^{-1}(\omega)]
$$

The linear part of the reset element needs to be added. The $D$ matrix does not have effect on all the harmonics, since this is outside the non linear part. To represent the $D$ matrix in the HOSIDF, it is added to the first harmonic.

It is concluded:

$$
\begin{aligned}
G(\omega,n) &= \begin{cases} C(j\omega I - A)^{-1}(I + j\Theta_D(\omega))B + D & \text{for } n = 1 \\ C(j\omega n I - A)^{-1} j\Theta_D(\omega) B & \text{for odd } n \geq 2 \\ 0 & \text{for even } n \geq 2 \end{cases} \\
\text{with } \Theta_D(\omega) &= -\frac{2\omega^2}{\pi}\Delta(\omega)[\Gamma_r(\omega) - \Lambda^{-1}(\omega)] \\
\Lambda(\omega) &= \omega^2 I + A^2 \\
\Delta(\omega) &= I + e^{\frac{\pi}{\omega}A} \\
\Delta_r(\omega) &= I + A_r e^{\frac{\pi}{\omega}A} \\
\Gamma_r(\omega) &= \Delta_r^{-1}(\omega) A_r \Delta(\omega) \Lambda^{-1}(\omega)
\end{aligned}
\tag{5-10}
$$

□

To verify the analytical solution, several simulations are done in Appendix A.

## 5-2 Visualization of the HOSIDF

The HOSIDF was calculated in the previous section. In order to be relevant for industry, it should be represented in the frequency domain like a Bode plot. In this section, we provide a visual frequency response of the higher order harmonics of the Clegg integrator.

When the system matrices of the Clegg integrator are plugged in Eq. (5-10), the HOSIDF for the Clegg integrator (CI) is obtained, as seen in Eq. (5-11). When the magnitude and phase are calculated per harmonic, the HOSIDF can be plotted. In Figure 5-3 the HOSIDF is plotted for the Clegg integrator. On the x-axis, the frequency of the sinusoidal input is seen. When the Clegg integrator is subjected to a sinusoidal input, several harmonics are created, because of the Virtual Harmonic Generator. The magnitude and phase behavior per harmonic order is plotted. It is noted that the Clegg integrator only has non-zero phase for the first order harmonic.

$$
\begin{aligned}
\text{for } n = 1 \qquad & CI(\omega) = \frac{1}{j\omega}(1 + j\frac{4}{\pi}) \\
\text{for odd } n \geq 2 \qquad & CI(\omega,n) = \frac{4}{\pi\omega n} \\
\text{for even } n \geq 2 \qquad & CI(\omega,n) = 0
\end{aligned}
\tag{5-11}
$$

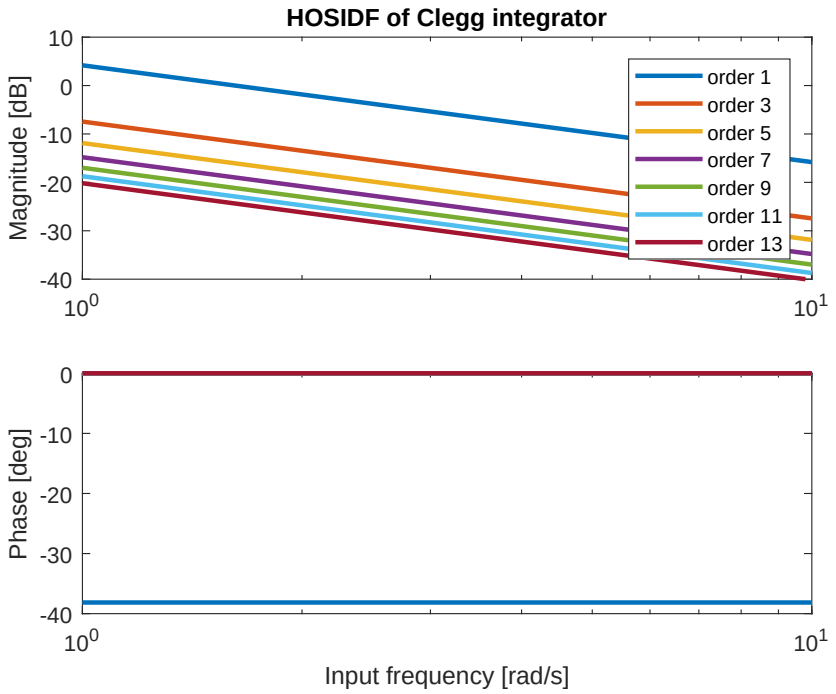


**Figure 5-3:** HOSIDF of Clegg integrator

## 5-3 Loop shaping

In linear feedback control, controllers can be designed using loop shaping. Closed loop stability is guaranteed as long as the system has an open loop positive phase margin. It is highly desired to apply the loop shaping method to reset systems. When the plant $P(s)$ is added after the controller, an analysis of the open loop system can be made, as seen in Figure 5-4.

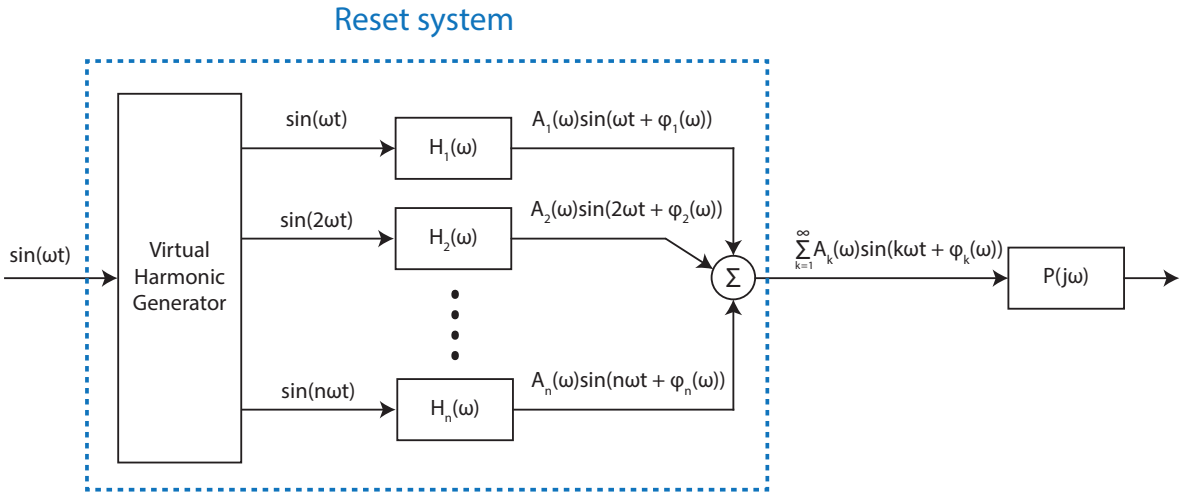


**Figure 5-4:** Block diagram of open loop reset controller and plant

Because of the additive property of controller blocks, the plant block $P(s)$ can be moved before the summation, as seen in Figure 5-5. It is seen that every harmonic of a reset system passes through a separate plant block. Each harmonic represents a different frequency, such that several frequencies are applied to the plant. The outputs of the plant blocks are summed up, creating an output consisting of sine waves which have properties depended on the reset controller and the plant.

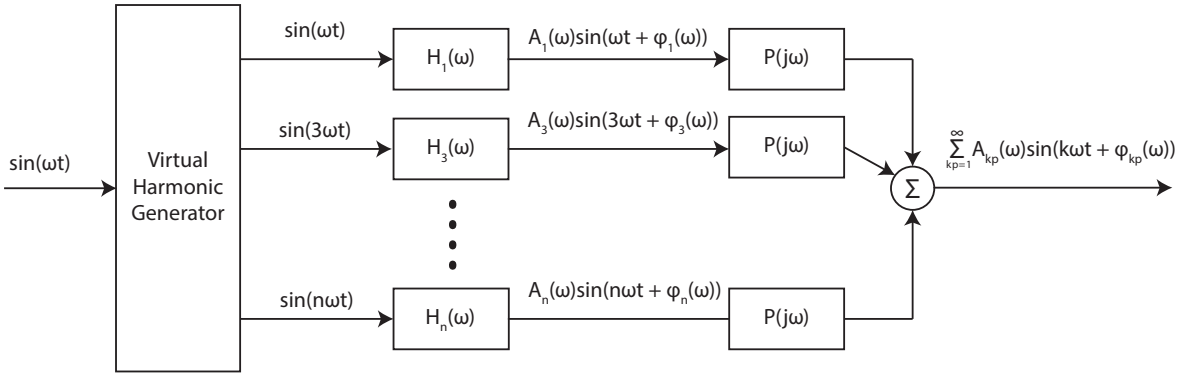


**Figure 5-5:** Block diagram of open loop reset controller and integrated plant

With Figure 5-5 in mind, the HOSIDF of the open loop system needs to be calculated as follows; For every harmonic, the phasor output of the reset controller is calculated, which results in a magnitude and phase. When inserting a 1 rad/s sine wave to a reset controller, a third harmonic is formed (which corresponds to a 3 rad/s sine wave). For the third harmonic (3 rad/s), the phasor output of the plant is calculated. The phasor output of the third harmonic of the reset controller and the plant are summed up. This is done for every harmonic $n$. This results in a open loop HOSIDF of:

$$L(\omega, n) = R(\omega, n)P(nj\omega) \tag{5-12}$$

### 5-3-1 Multiple peaks

It is noticed that multiple peaks occur in the open loop HOSIDF of a Clegg integrator and a mass spring damper (MSD) system. Consider an open loop HOSIDF which consists of a Clegg integrator and a MSD system, with natural frequency 10 rad/s and damping factor of 0.0125 (see Eq. (5-13)). In Figure 5-6 it is seen that the first order describing function shows a peak at 10 rad/s, which is the resonance frequency of the plant. The 3rd order shows a peak at 3.33 rad/s. The 5th order shows a peak at 2 rad/s. If an input frequency of 2 rad/s is considered, the 5th order represents a 10 rad/s sine wave. This frequency (10 rad/s) excites the resonance frequency in the plant, and therefore the 5th order shows a peak at 2 rad/s.

$$R(s) = \frac{1}{\cancel{s}} \qquad P(s) = \frac{100}{s^2 + 0.25s + 100} \tag{5-13}$$

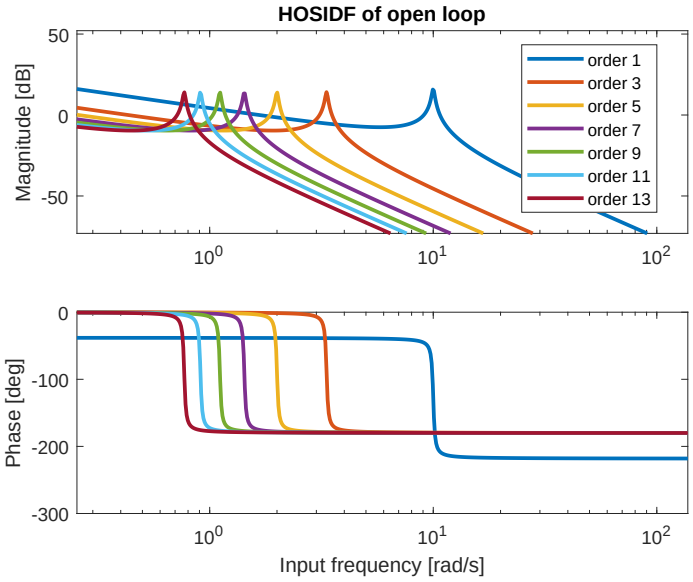


**Figure 5-6:** Open loop HOSIDF of Clegg integrator and MSD system

### 5-3-2 Analysis

Consider again the system from Eq. (4-3). This system has a stable closed loop step response (see Figure 4-4), but a negative phase margin, because of the inaccuracy of the first order describing function. With the HOSIDF, a new open loop frequency analysis can be made, as shown in Figure 5-7. It is clearly seen that all the higher orders have a positive phase margin, since their minimum phase is around -140°. It is suspected that the higher orders have a positive contribution to the phase margin, since the system behaves stable.

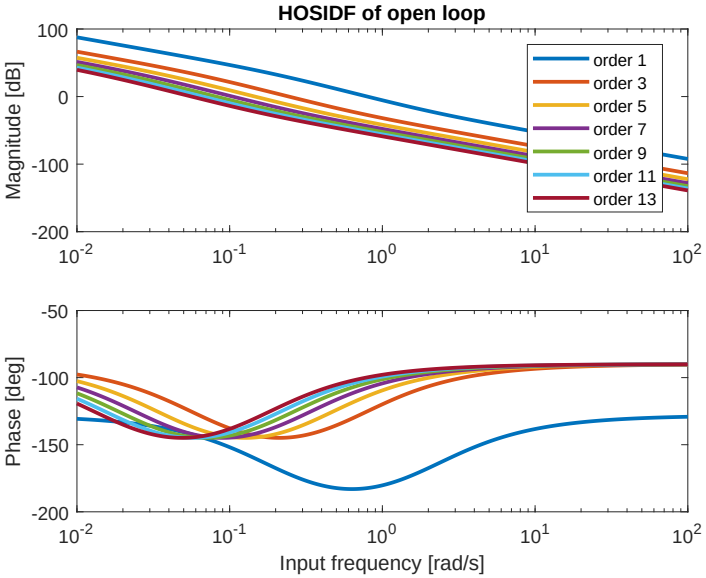


**Figure 5-7:** Open loop HOSIDF plot of Eq. (4-3)

In Section 4-3-1 it was suspected that the accuracy of the first order describing function was related to the gradient of the phase of the open loop system. With the HOSIDF, new insights can be obtained. Two MSD systems with different damping coefficients from Section 4-3-1 are simulated, both controlled by a Clegg integrator with a gain. Because they have different damping coefficients, they have a different gradient of phase. The gain is tuned such that the closed loop system performs marginally stable. In Figure 5-8a, a MSD system with $\zeta = 1.2$ is simulated. In Figure 5-8b, a MSD system with $\zeta = 0.0125$ is simulated.

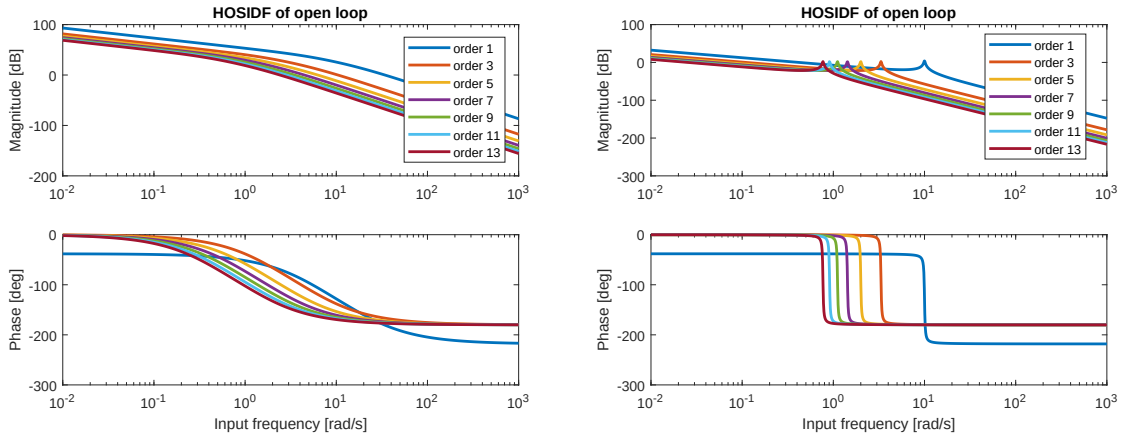


**(a)** MSD plant with $\zeta = 1.2$ **(b)** MSD plant with $\zeta = 0.0125$

**Figure 5-8:** Open loop HOSIDF of marginally stable MSD plants with different damping factors

It is seen that the higher order harmonics behave differently for both systems. For the MSD system with $\zeta = 1.2$, the crossover frequency for the first order is 33.5 rad/s. The third order has a magnitude of -30 dB and a phase of -166° at this frequency. For the MSD system with $\zeta = 0.0125$, the crossover frequency the the first order is 10.1 rad/s. The third order has a magnitude of -58 and a phase of -179.5° at this frequency. So when the damping is high, the magnitude of the third order lies closer to the first order than when the damping is low. This results in more contribution from the third order to the total system, making the first order describing function less accurate for the total system. This is in agreement with Section 4-3-1, where we concluded that for a MSD system with high damping, the first order describing function is less accurate than for MSD system with low damping.

It is seen that the higher order harmonics have some contribution to the phase margin. It is unclear yet how much they contribute. This will be researched in the next chapter.

## 5-4 Filtering effect of higher orders

When the plant has a pole at a certain frequency, the slope of the magnitude will decrease, and thus the magnitude will drop after this frequency. When the plant is controlled by a reset controller, a higher order harmonic will hit this pole frequency earlier, because of the properties discussed in the previous section. Because a higher order harmonic will hit the pole earlier, its magnitude will drop earlier as well. This will cause a filtering effect of the higher order harmonics.

Consider a plant $P(s)$ controlled by a Clegg integrator $R(s)$, as shown in Eq. (5-14). The plant has three poles located at 0.1 rad/s, 10 rad/s and 1000 rad/s. The open loop HOSIDF plot for this system is shown in Figure 5-9. It is seen that after each pole location, the distance between the harmonics increases.

$$R(s) = \frac{1}{\not{s}} \qquad P(s) = \frac{1}{(s+0.1)(s+10)(s+1000)} \tag{5-14}$$

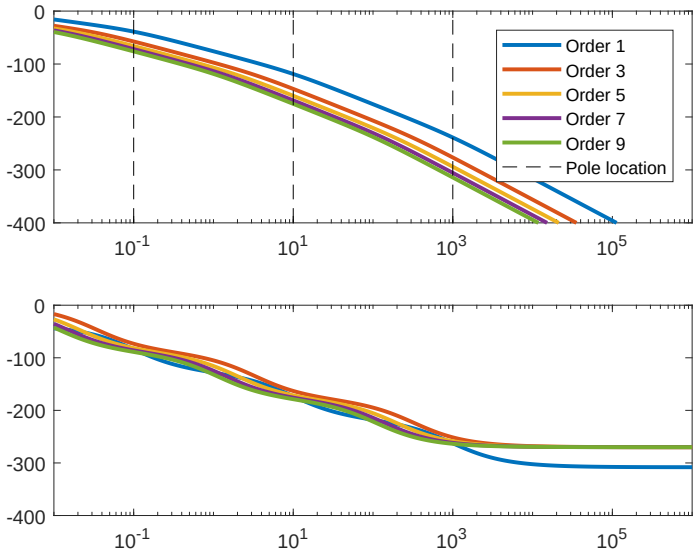


**Figure 5-9:** Filtering effect of the higher order harmonics

It is seen that magnitude line does not drop immediately after a pole location, but has some transient behavior which results in a smooth curvature. To know the 'steady state' distance of the harmonics, several new plants are created which consists of only pure integrators, as in Eq. (5-15). Pure integrators do not show transient behavior because their pole location is at $\omega = 0$. In Table 5-1 the distances are listed between the magnitude of the first and the third order describing function. It is seen that the distance linearly increases with 9.54 dB (0.333 in magnitude) if the plant has one more pole.

$$R(s) = \frac{1}{\not{s}} \qquad P_n(s) = \left(\frac{1}{s}\right)^n \tag{5-15}$$

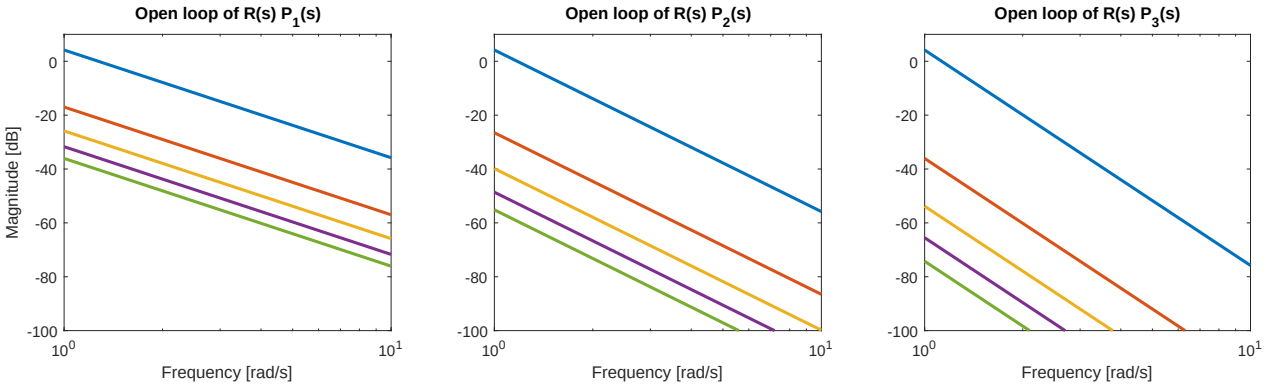


**Figure 5-10:** Open loop filtering effect of plants $P_1$ to $P_3$ controlled by a Clegg integrator

| Plant | Distance between 1st and 3rd order |
|---|---|
| $P_0$ | -11.63 dB |
| $P_1$ | -21.17 dB |
| $P_2$ | -30.71 dB |
| $P_3$ | -40.26 dB |
| $P_4$ | -49.80 dB |

**Table 5-1:** Distance between 1st and 3rd order harmonic per plant

# Chapter 6

# Combined HOSIDF

The HOSIDF is an useful tool to analyze reset systems. However, loop shaping is not trivial. Multiple harmonics show up in the HOSIDF, so it is e.g. unclear where the bandwidth frequency is located. It is desired to combine the higher order describing functions to form a single line for magnitude and phase, such that loop shaping can be achieved. Because the higher orders are combined, it is expected that this approach leads to more accurate results than the first order describing function.

In this chapter, a combined magnitude response is calculated by means of power in a signal. A combined phase response is calculated as well, which considers the algebraic phase between two vectors. It is seen that the combined phase shows jumps, such that loop shaping becomes inaccurate.

## 6-1 Magnitude

The closed loop bandwidth of a linear system is defined as the frequency where the closed loop output contains half the power of the input [29]. The magnitude part of the Bode plot represents the amplitude corresponding to the power throughput of a system. The power $P$ of a signal is defined as the energy measured over a certain time interval, as seen in Eq. (6-1) [30]. Linear systems consists of only pure sine waves, for which the power is calculated by Eq. (6-2). When the power of a sine wave is already known, its amplitude can be calculated by Eq. (6-3).

$$P_x = \frac{1}{T}\int_0^T |x(t)^2| dt \tag{6-1}$$

$$P_{\sin} = \frac{\omega}{2\pi}\int_0^{\frac{2\pi}{\omega}} \left|(A\ sin(\omega t))^2\right| dt = \frac{1}{2}A^2 \tag{6-2}$$

$$A = \sqrt{2P} \tag{6-3}$$

For linear systems, the power can be calculated from its sine wave amplitude, and this power can then be converted back to a corresponding amplitude. This is trivial, since the calculated amplitude is the same as the applied amplitude. However, for non linear systems (like reset systems) this approach will lead to new insights. The output of a reset systems is a summation of sine waves, as discussed in Chapter 5. When the output power is calculated, its corresponding sine wave amplitude can be calculated by Eq. (6-3). Dividing the output amplitude by its input amplitude creates a new combined magnitude line.

**Theorem 2.** *The combined magnitude line for a reset system is calculated as*

$$A_{combined}(\omega) = \sqrt{A_1(\omega)^2 + A_3(\omega)^2 + A_5(\omega)^2 + ...} \tag{6-4}$$

*Proof.* When a reset system is subjected to a sine wave input, the output consists of a summation of sine waves, as discussed in Chapter 5. The amplitudes and phases of these sine waves can be calculated with the HOSIDF. The output power is calculated by plugging the summation of sine waves in to Eq. (6-1).

$$\begin{aligned} P_y(\omega) &= \frac{\omega}{2\pi}\int_0^{\frac{2\pi}{\omega}} \Big|y(t)^2\Big| dt \\ &= \frac{\omega}{2\pi}\int_0^{\frac{2\pi}{\omega}} \Big(A_1(\omega)sin(\omega t + \phi_1(\omega)) + A_3(\omega)sin(3\omega t + \phi_3(\omega)) + A_5(\omega)sin(5\omega t + \phi_5(\omega)) + ...\Big)^2 dt \\ &= \frac{1}{2}\Big(A_1(\omega)^2 + A_3(\omega)^2 + A_5(\omega)^2 + ...\Big) \end{aligned} \tag{6-5}$$

To convert the output power to its corresponding amplitude, $P_y$ is plugged into Eq. (6-3).

$$A_y(\omega) = \sqrt{2P_y(\omega)} = \sqrt{A_1(\omega)^2 + A_3(\omega)^2 + A_5(\omega)^2 + ...} \tag{6-6}$$

Dividing the output amplitude $A_y$ by the input amplitude $A_u$ results in Eq. (6-7). Remember that the input signal was already a pure sine wave of amplitude 1.

$$A_{combined}(\omega) = \frac{A_y}{A_u} = \sqrt{A_1(\omega)^2 + A_3(\omega)^2 + A_5(\omega)^2 + ...} \tag{6-7}$$

□

It is noted from Eq. (6-7) that the combined magnitudes always lies higher than the magnitude of the first order describing function, since the higher order amplitudes are never zero.

### 6-1-1 Clegg integrator

The combined magnitude is plotted in the HOSIDF for the Clegg integrator in Figure 6-1. As can be seen, the combined magnitude lies slightly above the first order describing function.

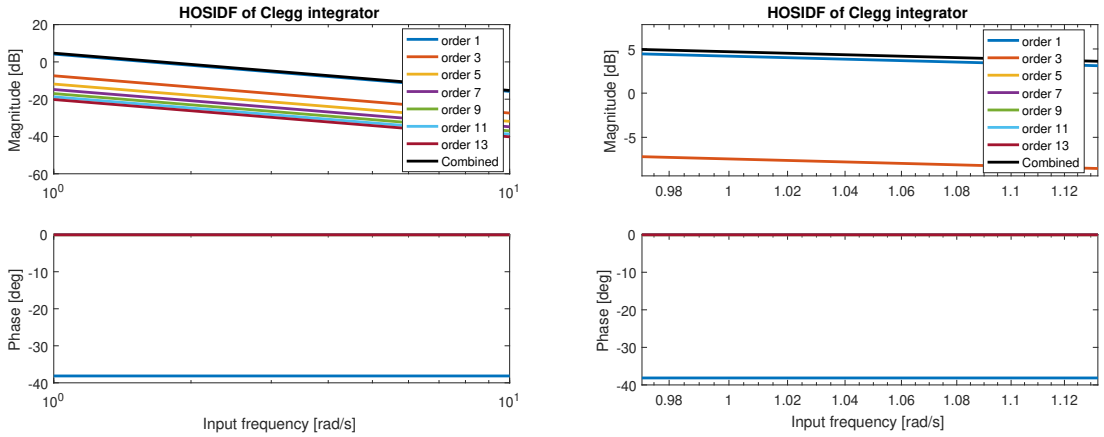


**(a)** HOSIDF with combined magnitude **(b)** Zoomed in

**Figure 6-1:** HOSIDF of Clegg integrator with combined magnitude

Every higher order harmonic for the Clegg integrator is of lower amplitude. When adding the higher orders to form the combined magnitude, the combined magnitude will therefore reach an asymptote. When the Clegg integrator is subjected to a 1 rad/s sine wave, the asymptote is $\sqrt{3} \approx 1.73$. This is proven in Appendix B-1. Because the magnitudes of the harmonics decreases evenly over the frequency spectrum, it does the same for the combined magnitude. The difference between the first order describing function magnitude and the combined magnitude is therefore constant. This constant difference is calculated in Eq. (6-8).

$$\frac{A_{\text{combined}}(\omega = 1)}{A_{\text{first order}}(\omega = 1)} = \frac{\sqrt{3}}{\sqrt{1 + \frac{16}{\pi^2}}} = 1.0698 = 0.5863 \text{ dB} \tag{6-8}$$

## 6-2 Phase

In the previous section, a combined magnitude was derived by looking at the power of the output. However, power tells nothing about the phase of a system. It is likely that the higher order harmonics have a contribution to the overall phase of the system. In this section, a new method is derived to analyze the phase of a reset system.

From linear algebra, it is known that the angle between vectors $u$ and $y$ can be expressed as Eq. (6-9). We are interested in the phase between an input signal $u(t) = sin(\omega t)$ and its corresponding reset system output, which is a summation of sine waves. In continuous time, the dot product and the 2-norm are defined in equation Eq. (6-10) for periodic signals, where $\overline{u(t)}$ is the complex conjugate of $u(t)$. $T$ is the fundamental time period of the signals.

$$\phi = cos^{-1}\left(\frac{y \cdot u}{\|y\|_2 \ \|u\|_2}\right) \tag{6-9}$$

$$y \cdot u = \frac{1}{T}\int_0^T y(t)\overline{u(t)}dt \qquad \|u\|_2 = \sqrt{\frac{1}{T}\int_0^T u(t)^2 dt} \tag{6-10}$$

**Theorem 3.** *The combined phase of a reset system is calculated as*

$$\phi_c(\omega) = cos^{-1}\left(\frac{A_1(\omega)}{\sqrt{A_1^2(\omega) + A_3^2(\omega) + A_5^2(\omega) + ...}}\ cos(\phi_1(\omega))\right) \tag{6-11}$$

*Proof.*

$$\phi_c = cos^{-1}\left(\frac{\frac{\omega}{2\pi}\int_0^{\frac{2\pi}{\omega}} y(t)\overline{u(t)}dt}{\sqrt{\frac{\omega}{2\pi}\int_0^{\frac{2\pi}{\omega}} y(t)^2dt}\ \sqrt{\frac{\omega}{2\pi}\int_0^{\frac{2\pi}{\omega}} u(t)^2dt}}\right) \tag{6-12}$$

$$\begin{aligned}\frac{\omega}{2\pi}\int_0^{\frac{2\pi}{\omega}} y(t)\overline{u(t)}dt =& \frac{\omega}{2\pi}\int_0^{\frac{2\pi}{\omega}} (A_1 sin(\omega t + \phi_1) + A_3 sin(3\omega t + \phi_3) + A_5 sin(5\omega t + \phi_5) + ...)sin(\omega t))dt \\ =& \frac{\omega}{2\pi}\int_0^{\frac{2\pi}{\omega}} A_1 sin(\omega t + \phi_1)sin(\omega t)dt + \\ & \frac{\omega}{2\pi}\int_0^{\frac{2\pi}{\omega}} A_3 sin(3\omega t + \phi_3)sin(\omega t)dt + \\ & \frac{\omega}{2\pi}\int_0^{\frac{2\pi}{\omega}} A_5 sin(5\omega t + \phi_5)sin(\omega t)dt\ + ...\end{aligned} \tag{6-13}$$

There are infinite harmonics, so this results in infinite integrals. This can be reduced to solving two integrals, one for the first harmonic, and one for harmonic $n$, where $n$ is odd and higher than 2. Only the odd harmonics are relevant, since the even harmonics are zero.

$$\begin{aligned}\int_0^{\frac{2\pi}{\omega}} A_1 sin(\omega t + \phi_1)sin(\omega t)dt &= \frac{\pi A_1 cos(\phi_1)}{\omega} \\ \int_0^{\frac{2\pi}{\omega}} A_n sin(n\omega t + \phi_n)sin(\omega t)dt &= 0 \quad (\text{for odd } n > 2)\end{aligned} \tag{6-14}$$

$$\frac{\omega}{2\pi}\int_0^{\frac{2\pi}{\omega}} y(t)\overline{u(t)}dt = \frac{\omega}{2\pi}\frac{\pi A_1 cos(\phi_1)}{\omega} \tag{6-15}$$

The 2-norms are calculated as follows:

$$\sqrt{\frac{\omega}{2\pi}\int_0^{\frac{2\pi}{\omega}} u(t)^2dt} = \sqrt{\frac{\omega}{2\pi}\int_0^{\frac{2\pi}{\omega}} sin(\omega t)^2dt} = \sqrt{\frac{\omega}{2\pi}\frac{\pi}{\omega}} \tag{6-16}$$

$$\begin{aligned}\sqrt{\frac{\omega}{2\pi}\int_0^{\frac{2\pi}{\omega}} y(t)^2dt} &= \sqrt{\frac{\omega}{2\pi}\int_0^{\frac{2\pi}{\omega}} (A_1 sin(\omega t + \phi_1) + A_3 sin(3\omega t + \phi_3) + A_5 sin(5\omega t + \phi_5) + ...)^2dt} \\ &= \sqrt{\frac{\omega}{2\pi}\frac{\pi(A_1^2 + A_3^2 + A_5^2 + ...)}{\omega}}\end{aligned} \tag{6-17}$$

Combining the results will lead to the final phase equation.

$$\begin{aligned}\phi_c(\omega) &= cos^{-1}\left(\frac{\frac{\omega}{2\pi}\int_0^{\frac{2\pi}{\omega}} y(t)\overline{u(t)}dt}{\sqrt{\frac{\omega}{2\pi}\int_0^{\frac{2\pi}{\omega}} y(t)^2dt}\sqrt{\frac{\omega}{2\pi}\int_0^{\frac{2\pi}{\omega}} u(t)^2dt}}\right)\\ &= cos^{-1}\left(\frac{\frac{\pi A_1(\omega)cos(\phi_1(\omega))}{\omega}}{\sqrt{\frac{\pi}{\omega}}\sqrt{\frac{\pi(A_1^2(\omega)+A_3^2(\omega)+A_5^2(\omega)+...)}{\omega}}}\right)\\ &= cos^{-1}\left(\frac{A_1(\omega)}{\sqrt{A_1^2(\omega)+A_3^2(\omega)+A_5^2(\omega)+...}}cos(\phi_1(\omega))\right)\end{aligned} \tag{6-18}$$

□

It is noted that the combined phase is not depended on the phases of the higher order harmonics, but on the amplitudes of the higher order harmonics. When the higher order amplitudes are of low magnitude, the combined phase lies close to the phase of the first order describing function.

It is also noted that the phase of the first order describing function ($\phi_1$) is inserted in the cosine function. A cosine function is periodic, and therefore returns the same value for e.g. -170°, 170° and -190°. When these numbers are plugged in the inverse cosine, 170° is returned. This way, information about the quadrant is lost. Algorithm 1 is implemented after the combined phase calculation, to compensate for the the lost quadrant information.

b := floor($\phi_1$/180°);
**if** *b is divisible by 2* **then**
  $\phi_c$ = 180°b + $\phi_c$;
**else**
  $\phi_c$ = 180°(b+1) - $\phi_c$;
**end**

**Algorithm 1:** Quadrant compensation for the combined phase

### 6-2-1 Clegg integrator

The combined phase is plotted in the HOSIDF for the Clegg integrator in Figure 6-1a. As can be seen, the combined phase lies below to the first order describing function. In Appendix B-2 it is shown that the combined phase is -42.68°. This is 4.44° lower then the first order describing function.

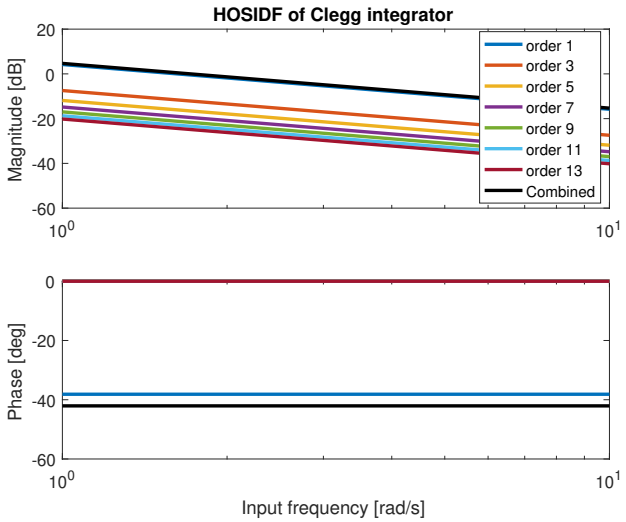


**Figure 6-2:** HOSIDF of Clegg integrator with combined magnitude and phase

### 6-2-2 Jump behavior

The combined phase looks interesting, but there is a problem. Consider a system which consists of a Clegg integrator $R(s)$ controlling a mass damper system $P(s)$, as in Eq. (6-19). Its HOSIDF is plotted in Figure 6-3. It is seen that the combined phase has a jump around 1.27 rad/s, such that there is no frequency where the phase is exactly -180°. This is incorrect, since this would mean that a reset system cannot be unstable. It is also noticed that the combined phase drifts away from the first order phase around 1.27 rad/s. For frequencies much lower or higher, the combined phase is almost equal to the first order phase.

$$R(s) = \frac{1}{s^{\nearrow}} \qquad P(s) = \frac{1}{s^2 + s} \tag{6-19}$$

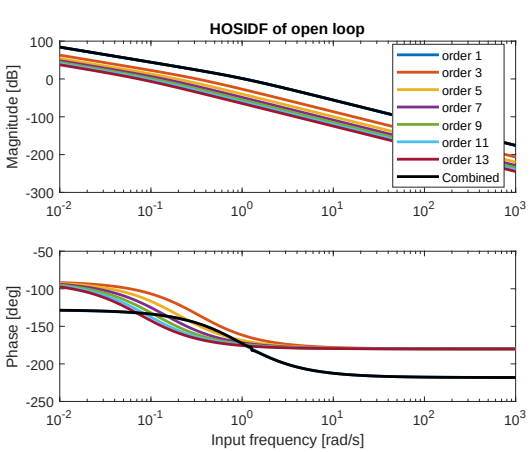


**(a)** HOSIDF with jump in combined phase

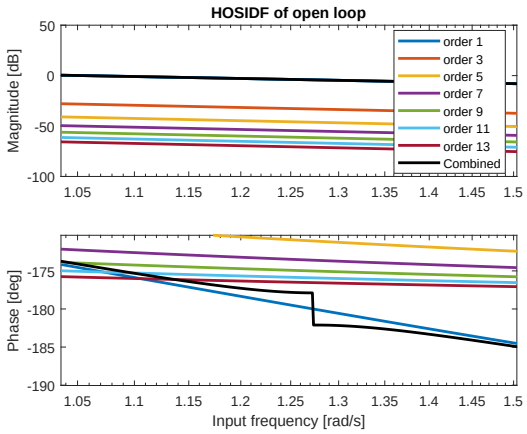


**(b)** HOSIDF with jump in combined phase, zoomed in

**Figure 6-3:** HOSIDF with jump in combined phase

The jump happens because the output of the cosine of the phase of the first order describing function is multiplied with an amplitude. This amplitude is always smaller than 1, while the output of a cosine is always between -1 and 1. When the amplitude is 0.999, the multiplication of both will lie between -0.999 and 0.999. When taking the inverse cosine of this, the result is between 2.5° and 177.5°. In other words, there is no smooth behavior going from -170° to -190°. This results in a phase jump around -180°.

The phase jump can also be explained in a graphical way. Consider Figure 6-4, where two points on the unit disk are drawn, such that both the hypotenuses are 1. Point $P_1$ has an angle $\phi_1$ and an adjacent side of $a_1$. Point $P_2$ has an angle $\phi_2$ and an adjacent side of $a_2$, which is always a fraction smaller (0.99) than $a_1$, so $a_2 = 0.99a_1$. Because of the latter, there is always a horizontal distance $d$ between $P_1$ and $P_2$. When $\phi_1$ is exactly 0°, the point $P_1$ lays on the intersection of the unit circle and the x-axis. Because $d$ remains non zero and both the hypotenuses remain 1, $P_2$ has to be above or below the x-axis. When $\phi_1$ is smoothly lowered such that $P_1$ goes through the x-axis, $P_2$ will follow with a jump.

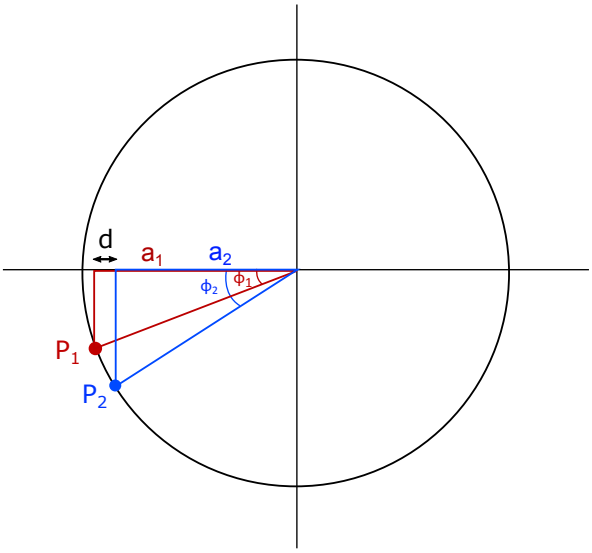


**Figure 6-4:** Unit circle showing two points with a non zero adjacent distance

Consider the case where the combined phase is calculated for a certain frequency. This will result in Eq. (6-20).

$$\phi_c = cos^{-1}\left(\frac{A_1}{\sqrt{A_1^2 + A_3^2 + A_5^2 + ...}}\, cos(\phi_1)\right) \tag{6-20}$$

When calculating a cosine of an angle, the adjacent side is returned (assuming a hypotenuse of 1). So in case of the combined phase, $a_1 = cos(\phi_1)$. The output of this cosine is however multiplied with an amplitude, creating an adjacent side of a different length ($a_2$). When the inverse cosine is taken from this adjacent side, an angle is returned (assuming a hypotenuse of 1). In case of the combined phase for the HOSIDF, the distance $d$ is given by Eq. (6-21). The value for $d$ will never be zero, so a jump will always occur.

$$d = a_1 - a_2 = cos(\phi_1) - \frac{A_1}{\sqrt{A_1^2 + A_3^2 + A_5^2 + ...}} cos(\phi_1) = cos(\phi_1) \left( 1 - \frac{A_1}{\sqrt{A_1^2 + A_3^2 + A_5^2 + ...}} \right) \tag{6-21}$$

## 6-3 Loop shaping

In the previous two sections, a new magnitude and phase approach has been created for reset systems. The new approach takes the higher order harmonics into account, which can lead to more accurate results. In this section, the results of the combined magnitude and phase are discussed. This is done by applying loop shaping for mass spring damper (MSD) systems with and without damping. We also discuss the accuracy of loop shaping with the combined magnitude and phase.

### 6-3-1 Mass spring damper system without damping

Consider a Clegg integrator $R(s)$ controlling a plant $P(s)$, as in Eq. (6-22). The plant $P(s)$ is a MSD system with a natural frequency of 1 rad/s and no damping, such that the resonance frequency has infinite gain. The HOSIDF is plotted in Figure 6-5, with the combined magnitude and phase.

$$R(s) = \frac{1}{s} \qquad P(s) = \frac{1}{s^2 + 1} \tag{6-22}$$

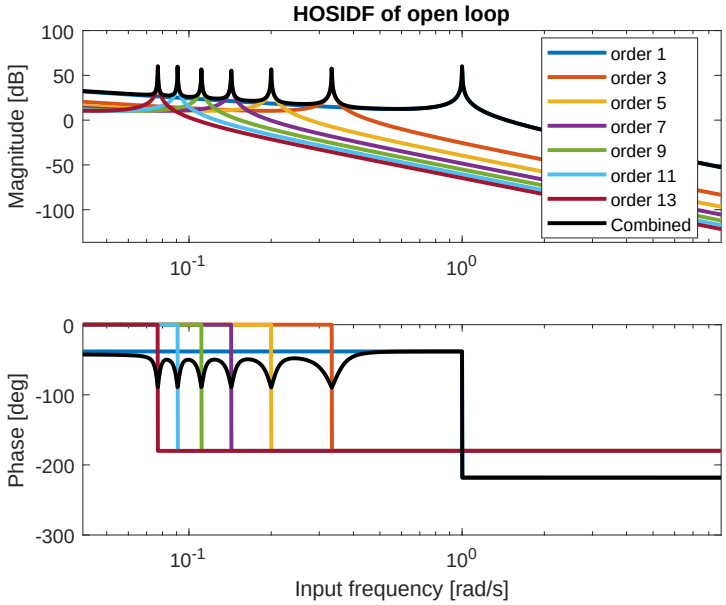


**Figure 6-5:** HOSIDF with combined magnitude and phase of MSD system with no damping, controlled by a Clegg integrator

In Figure 6-5 it is seen that multiple resonance frequencies appear in the combined magnitude response. Each harmonic hits the resonance frequency of the plant (as discussed in Section 5-3), and therefore has infinite gain as well. The harmonics are added up to form the combined magnitude, which as a result has multiple infinite gain peaks. The infinite gain peaks from the harmonics can be seen in the time domain as well. In Figure 6-6a, the system is excited in open loop by a sine wave of 0.2 rad/s. At this frequency, the fifth order hits the resonance frequency of the plant. In the time domain it is seen that the output grows, indicating a infinite steady state amplitude. In Figure 6-6b, the system is excited by a sine wave of 0.6 rad/s. This frequency is not related to a harmonic resonance, and therefore does not grow in the time domain. These time domain simulations verify the combined magnitude line of the HOSIDF. The multiple peaks are not captured by the first order describing function, indicating that the combined magnitude shows more accurate information than the first order describing function.

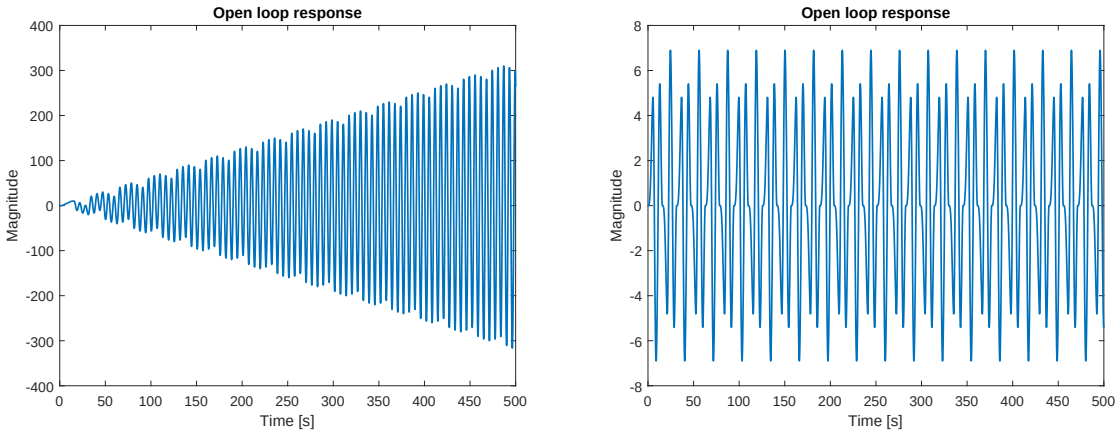


**(a)** Open loop response of $u(t) = sin(0.2t)$ **(b)** Open loop response of $u(t) = sin(0.6t)$

**Figure 6-6:** Open loop time domain responses of MSD system with zero damping

It is noted that the combined phase has no jump behavior at the crossover frequency in Figure 6-5. This is because the magnitude at crossover frequency has infinite gain, making the combined phase equal to the phase of the first order describing function. It is also noted that the combined phase has a dip at every resonance frequency. This happens because at a harmonic resonance frequency, the harmonic has infinite gain. When this infinite gain is insert in Eq. (6-11), the output is $\phi_c = cos^{-1}(0 \cdot cos(\phi_1)) = -90°$

As discussed before, the combined magnitude lies always higher than the first order describing function. If the plot is recreated with more harmonics for a low frequency range, Figure 6-7 is obtained. In this plot, only the first order and the combined phase are listed in the legend. The shown peaks are the higher order harmonics. It is seen that the minimum of the combined magnitude lies $\sim$2 dB higher than the first order describing function. High magnitude in the low frequency range implies good tracking. Because the combined phase lies higher than the first order describing function, it may give better tracking performance than what was expected by the first order describing function.

It is also seen that the phase makes multiple jumps between -50° and -90°. At a harmonic resonance frequency, the gain of the harmonic is infinite, so the combined phase goes to -90°.

The minimum phase stays however around -50°, which is lower than the -38° of the first order describing function.

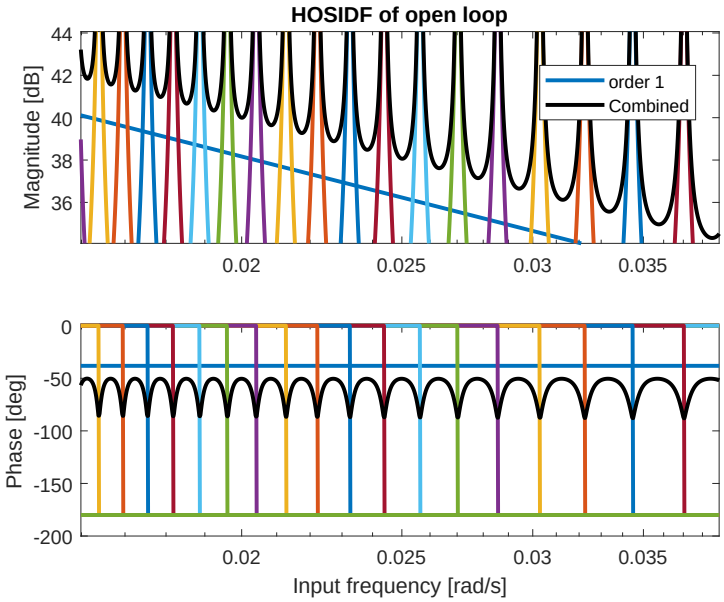


**Figure 6-7:** Zoomed in HOSIDF of MSD with no damping showing many harmonics

### 6-3-2 Mass spring damper system with damping

Systems with zero damping are hard to find in practice. In the next example, a mass spring damper (MSD) system with little damping is considered.

A MSD system is controlled by a Clegg integrator, as in Eq. (6-23). The HOSIDF is plotted in Figure 6-8. It is seen from the HOSIDF plot that the combined magnitude lies higher than the first order describing function for low frequencies. For MSD systems without damping, this offset was around 2 dB. For this MSD system, the offset is around 1 dB. The resonance peaks for a MSD with damping are lower in magnitude, such that the combined magnitude is lower in magnitude as well. This makes the offset between the combined magnitude and the first order describing function less. When more damping is added, the peaks are even further lowered, creating an even lower offset between the combined magnitude and the first order describing function.

The combined phase has small dips where the harmonic resonance frequencies are. The maximum phase in the low frequency region is no longer -50°, but comes closer to -42.68°, which is the combined phase of a Clegg integrator. When more damping is added, the combined phase will approach the combined phase of the Clegg integrator.

$$R(s) = \frac{1}{\cancel{s}} \qquad P(s) = \frac{1}{s^2 + 0.1s + 1} \tag{6-23}$$

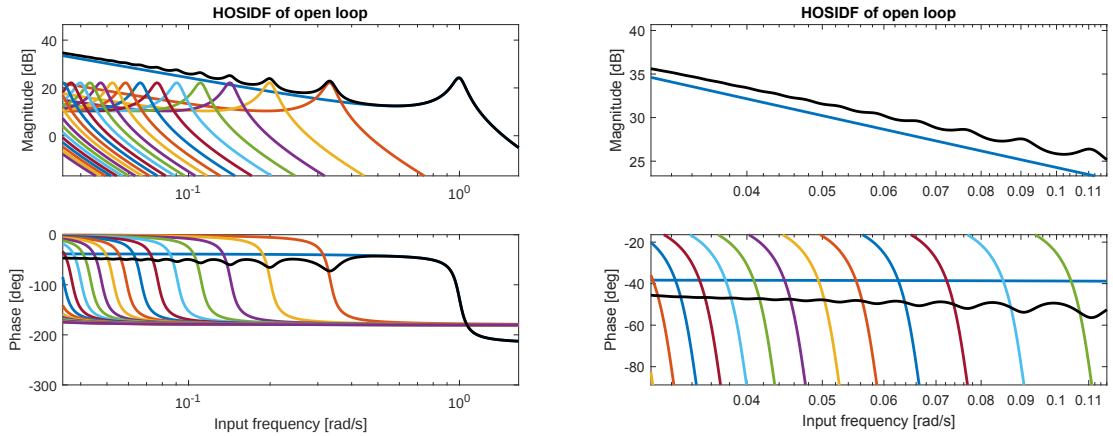


**(a)** HOSIDF of Eq. (6-23)

**(b)** HOSIDF of Eq. (6-23), zoomed in

**Figure 6-8:** HOSIDF of MSD system with little damping controlled by a Clegg integrator from Eq. (6-23)

The combined phase in Figure 6-8 has a jump where the first order describing function passes -180°, although this is not clearly visible. If more damping is added, the higher orders will lie more close to the first order describing function around the crossover frequency. This makes the distance $d$ from Section 6-2-2 bigger, so a bigger jump occurs. The combined phase jump will lead to inaccurate results, as will be discussed in the next section.

### 6-3-3 Accuracy of combined HOSIDF

In Section 4-3-1, it was seen that loop shaping was not accurate if the first order describing function was considered. In this chapter, the HOSIDF was combined to form a single response for magnitude and phase. In this section, we investigate if the combined HOSIDF shows more accurate results.

Consider a MSD system ($\omega_n = 10$, $\zeta = 1.2$) which is controlled by a Clegg integrator with a gain, as in Eq. (6-24). This is the same system as in Section 4-3-1, so the gain is chosen such that the system is marginally stable. In Figure 6-9, the HOSIDF is plotted for this system. The zoomed in HOSIDF is shown in Figure 6-9b and considers only the first order describing function and the combined magnitude and phase response. It is seen that the magnitude of the first order describing function and the combined magnitude is close to each other. The crossover frequency is determined from the combined magnitude and is plotted in Figure 6-9b. The combined phase shows a jump of 4° around 33.5 rad/s. This results in a large offset between the combined phase and the phase of the first describing function at the crossover frequency.

In Section 4-3-1, it was calculated that the first order describing function had a phase of -180.6° around the crossover frequency. This was however calculated with the crossover frequency of the first order describing function. The magnitude response of the first order describing function is however so close to the combined magnitude, that it is not relevant which magnitude response we chose to determine the crossover frequency. The combined phase is -182° around the crossover frequency, which is further away from -180° than -180.6°.

$$R(s) = \frac{K}{\not{s}} \qquad P(s) = \frac{\omega_n^2}{s^2 + 2\zeta\omega_n s + \omega_n^2} \tag{6-24}$$

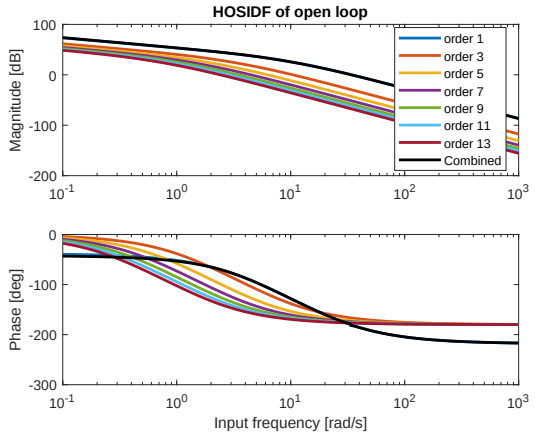


**(a)** HOSIDF of MSD system

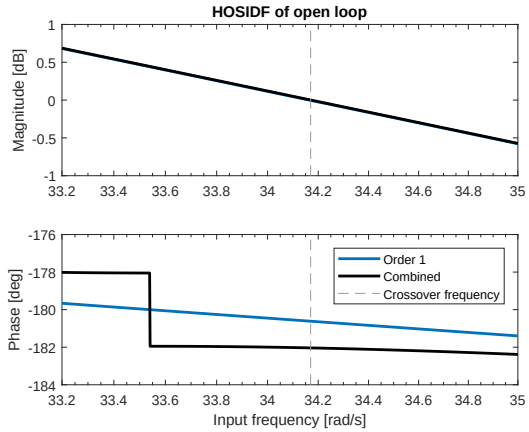


**(b)** Zoomed in HOSIDF, combined response calculated with 50 orders

**Figure 6-9:** HOSIDF of marginal stable MSD system controlled by a Clegg integrator with combined magnitude and phase

To summarize, the combined phase predicts a more inaccurate result than the first order describing function. If more damping is added to the system, the jump from the combined magnitude increases, and thus creating a big offset.

It is seen that the combined magnitude shows promising results, because it captures the harmonic resonances. The combined phase however encounters a jump when the first order describing function passes -180°. This makes the result from the combined phase inaccurate. The combination of magnitude and phase needs to match to test for marginal stability. For marginal stable systems, the frequency where the magnitude crosses 0 dB should be the same frequency where the phase crosses -180°. A new method for magnitude and phase analysis is created, but this can not be verified with the marginal stability test if the new phase response is inaccurate. It is concluded that the combined magnitude and phase is not mature enough yet to rely on during loop shaping.

# Chapter 7

# Discussion

The HOSIDF is a promising way of analyzing reset systems. Not every aspect of the HOSIDF could be analyzed, and therefore there are topics which could be researched further.

## 7-1 Rules of thumb design

With the HOSIDF, a tool is created which gives much more insight is given for reset systems. For similar first order describing functions, the higher harmonics can be different. Because the higher order harmonics can now be analyzed, new design rules can be made for reset systems. It is desired to have some rules of thumb to design reset systems.

## 7-2 Analytical stability solution

In Section 3-4 a stability criterion was shown. With this criterion, reset systems can be proven to be (un)stable, when the reset interval $\tau$ was known. The reset interval was simulated with Simulink, instead of calculating it analytically. Therefore, computational errors could occur. The stability analysis would be more accurate if the reset interval was calculated instead of simulated.

## 7-3 Combined phase jump

It was seen in Section 6-2-2 that the combined phase has jumps when the first order describing function passes -180°. There is no frequency where the combined phase is exactly -180°. If the magnitude is higher than 0 dB at the -180°, the system will become unstable. If the phase is never -180°, a reset system can not be unstable. There are however many examples of unstable reset systems. This concludes that the combined phase is not correct, and further research needs to be done.

This thesis considered only jumps which happened when the first order describing function was -180°, but jumps happens at every $n \cdot 180°$ with $n \in \mathbb{Z}$.

## 7-4 Closed loop HOSIDF

Stability and performance analysis is done in open loop, and therefore only the open loop HOSIDF have been considered. Calculating the closed loop HOSIDF is not as trivial as for linear systems. A linear integrator in open loop will become a first order element when closing the loop. A Clegg integrator in open loop will however not become a FORE in closed loop. The closed loop response of a Clegg integrator is plotted in Figure 7-1a. In 7-1b the Fourier transformation is plotted. It is seen that the amplitude of harmonics do not always decrease when the harmonic order increases. The 7th order harmonic appears to be slightly higher than the 5th order.

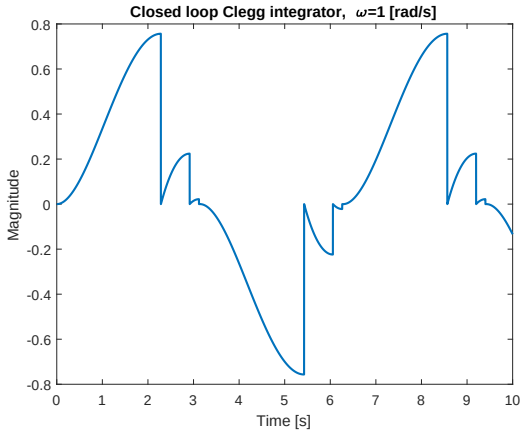


**(a)** Closed loop response for $\omega = 1$ rad/s

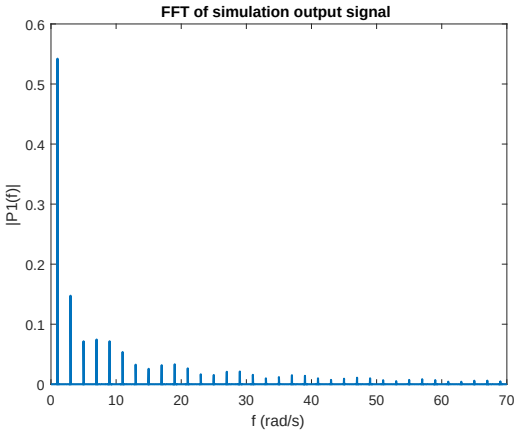


**(b)** FFT of closed loop Clegg integrator $\omega = 1$ rad/s

**Figure 7-1:** Closed loop response of Clegg integrator

The open loop HOSIDF $L(\omega, n)$ is known for every harmonic. When each harmonic is inserted in Eq. (7-1), the closed loop HOSIDF in Figure 7-2 is obtained. It can be seen here that all the harmonic magnitudes are decreasing if the order increases. In this plot, the 7th order harmonic is not higher than the 5th. This is in contrast with the Fourier transformation seen in Figure 7-1b.

$$T(\omega, n) = \frac{L(\omega, n)}{1 + L(\omega, n)} \tag{7-1}$$

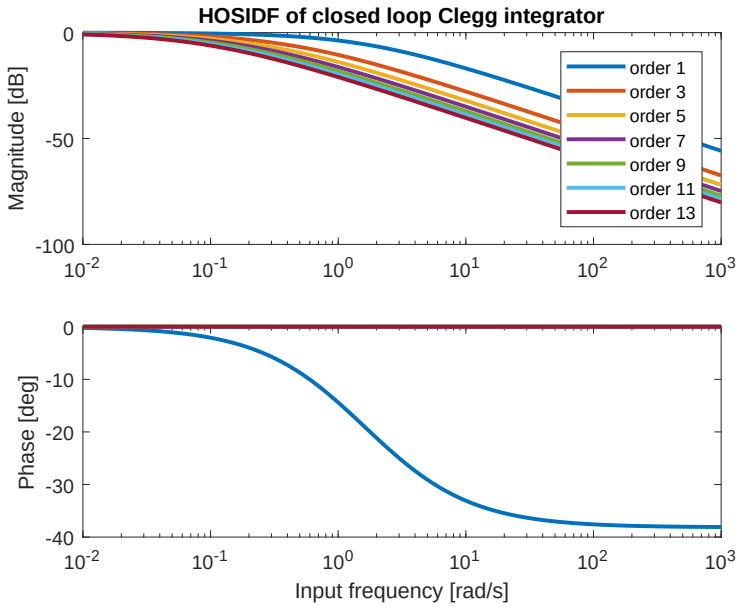


**Figure 7-2:** HOSIDF of closed loop Clegg integrator

It is clear that the closed loop HOSIDF plot from Figure 7-2 is incorrect. The plot was created using Eq. (7-1), which calculates the closed loop per harmonic. This way, the closed loop HOSIDF does not take the harmonic influences on each other into account. It is suspected that in feedback, the harmonics have some sort of interaction with each other. Further research needs to be done about this topic.

## 7-5 Closed loop stable sinusoidal input

If a linear system is unstable, every input will result in a unstable closed loop response. If a reset system is unstable, not every input will result in instability.

Consider a system with a Clegg integrator and a plant $P(s) = 0.11\frac{s+2}{s^2+0.2s}$. This system has an unstable closed loop step response. However, if a sine wave is applied to the closed loop system, it depends on the input frequency if the output is unstable or not. With simulation it is found that for this system, a frequency up to 0.71039 rad/s gives an unstable response. Any frequency higher than this gives a stable response. When the plant is changed to $P(s) = \frac{4}{s^2+s+1}$, the same behavior occurs for an input frequency up to 2.0628 rad/s.

This is unexpected behavior and further research needs to be done.

# Chapter 8

# Conclusion

The research goal of this study was to:

*Integrate higher order information into a frequency domain representation for the analysis of reset systems containing a Clegg integrator.*

First, an introduction was given to reset systems. Reset control can overcome fundamental limitations of linear control, which could lead to better results. It was shown that linear controllers are designed in the frequency domain using loop shaping. Reset systems are hard to represent in the frequency domain since they are non linear. Their frequency response needs to be approximated using describing functions. The current state of the art uses only first order describing functions. It was proven with a stability condition that the first order describing function is not accurate. The inaccuracy was however in our favor, because the describing function predicted instability for stable systems. Current describing function analysis did not give accurate results, so higher order needed to be considered.

The HOSIDF has been introduced, which gives better insight of reset elements in the frequency domain, because it considers the higher order dynamics. The HOSIDF shows magnitude and phase behavior per harmonic, such that performance and stability could be investigated more accurate. Because the HOSIDF shows multiple responses, it is not trivial how to do loop shaping.

A new method for analyzing the magnitude and phase behavior of a reset system has been proposed, by combining the information from the HOSIDF to form a single response for magnitude and phase. It was seen that the combined magnitude seems promising, since resonance frequencies were clearly seen in the low frequency spectrum. However, the combined phase showed a jump where the first order describing function passed -180°. This jump leads to inaccurate results. It is concluded that the combined magnitude and phase approach is not mature enough, and further research needs to be done in this direction.

# Appendix A

# HOSIDF verification results

The HOSIDF was found analytically so it should match the output of a reset element. It is still desired to verify the results to see if no errors are made during the derivation.

One way to verify the results is to simulate the response of a sine wave input to a reset system. When taking the Fourier series of the system output, one should see the harmonics of the output signal. The amplitude of these harmonics should match the results from the calculated HOSIDF.

Several reset systems are tested; a Clegg integrator, a first order reset element (FORE), a P+CL controller, a partial reset Clegg integrator and a Clegg integrator controlling a plant. All simulations are done in the same way: A sine wave of 10 rad/s and amplitude 1 is excited to the system. The output will be simulated in Simulink and Fourier transformed with the 'FFT' command in MATLAB. The sample frequency is chosen to be 200 samples per period, to avoid aliasing. The simulation time is such that there are exactly 500 periods, to avoid spectral leakage. This results in a sampling time of 3.141 ms and a simulation time of 314.159 s.

## A-1 Clegg integrator

$$R(s) = \frac{1}{s} \tag{A-1}$$

A Clegg integrator (Eq. (A-1)) is simulated in open loop, as seen in Figure A-1a. Note that in Figure A-1a, only 2 seconds are shown, for displaying purposes. The simulated output is Fourier transformed with the Fast Fourier Transform (FFT), which can be seen in Figure A-1b.

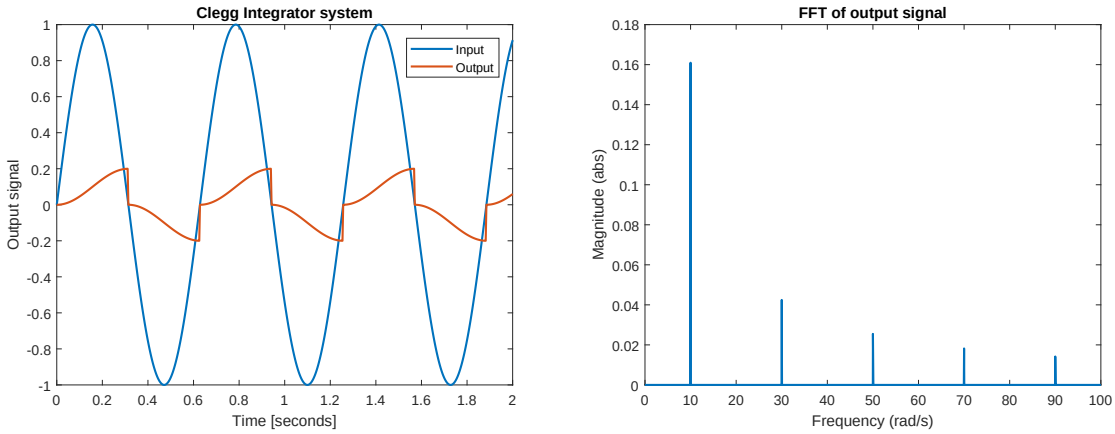


**(a)** Zoomed in/output signal of Clegg integrator **(b)** Zoomed in view of FFT of output signal

**Figure A-1:** Clegg integrator time domain simulation with corresponding Fourier transform

As can be seen in Figure A-1b, the FFT shows a big peak at 10 rad/s, which is the base frequency ($1^{\text{st}}$ harmonic). At 20 rad/s (the $2^{\text{nd}}$ harmonic) the FFT is zero, as expected. At 30 rad/s ($3^{\text{rd}}$ harmonic) the FFT has a much lower peak value than the first harmonic. The FFT magnitudes are compared to the amplitudes of the HOSIDF. To calculate the HOSIDF, the transfer function from Eq. (A-1) has to be converted to a state space representation, which is done in Eq. (A-2). The resulting HOSIDF is shown in Figure A-2a. In Figure A-2b, the magnitude plot is zoomed in and the y-axis displays the magnitude in absolute value, instead of decibels.

$$\left.\begin{array}{c|c} A & B \\ \hline C & D \end{array}\right. = \left.\begin{array}{c|c} 0 & 1 \\ \hline 1 & 0 \end{array}\right. , \qquad A_r = 0 \tag{A-2}$$

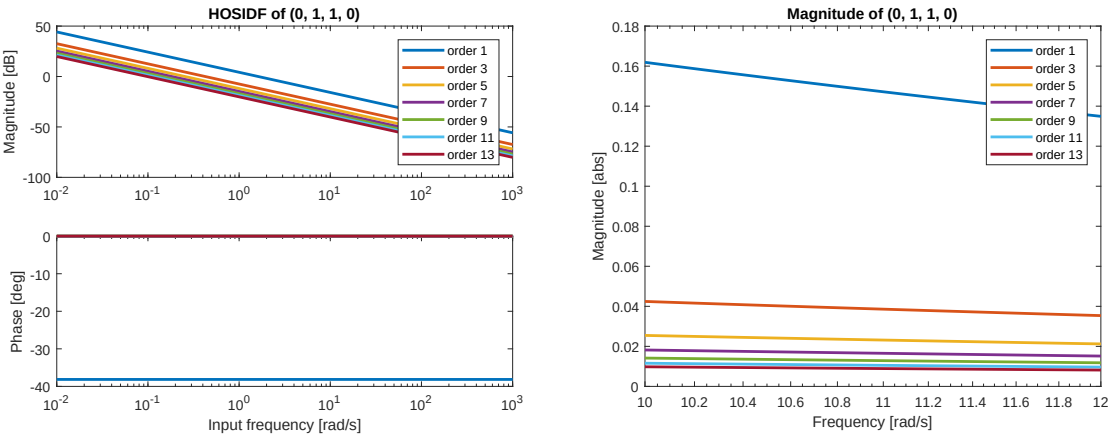


**(a)** HOSIDF of Clegg integrator **(b)** Zoomed HOSIDF around 10 rad/s

**Figure A-2:** HOSIDF of Clegg integrator

**Table A-1:** Comparison of FFT results with HOSIDF

| Order | FFT Mag | HOSIDF Mag | Error in % |
|---|---|---|---|
| 1 | 0.1610 | 0.1619 | 0.5844 |
| 3 | 0.0425 | 0.0424 | 0.0361 |
| 5 | 0.0255 | 0.0255 | 0.1019 |
| 7 | 0.0182 | 0.0182 | 0.2008 |
| 9 | 0.0142 | 0.0141 | 0.3329 |
| 11 | 0.0116 | 0.0116 | 0.4984 |
| 13 | 0.0099 | 0.0098 | 0.6974 |
| 15 | 0.0086 | 0.0085 | 0.9304 |
| 17 | 0.0076 | 0.0075 | 1.1975 |
| 19 | 0.0068 | 0.0067 | 1.4992 |
| 21 | 0.0062 | 0.0061 | 1.8359 |
| 23 | 0.0057 | 0.0055 | 2.2081 |
| 25 | 0.0052 | 0.0051 | 2.6163 |

The magnitudes of the FFT are compared to the calculated amplitudes from the HOSIDF. As can be seen in Table A-1, the FFT and the HOSIDF are almost the same. The small error is due to the calculation of the FFT, which always has computational errors, although small. When calculating the FFT with higher sampling frequency and a longer experiment time, the error gets smaller. This highly indicates that the FFT is not a perfectly accurate method. Because of this, the error increases for higher orders.

The same experiment is repeated for a FORE, a P+CL controller, a partial reset Clegg integrator and a Clegg integrator controlling a plant. These can be found in the next sections. Because the method is the same for the other sections, only the results are shown.

## A-2 FORE

An open loop first order reset element $R(s)$ is simulated.

$$R(s) = \frac{1}{\cancel{s+10}} \tag{A-3}$$

**Table A-2:** Comparison of FFT results with HOSIDF for a FORE

| Order | FFT Mag | HOSIDF Mag | Error in % |
|---|---|---|---|
| 1 | 0.8347 | 0.8357 | 0.1161 |
| 3 | 0.1058 | 0.1050 | 0.7195 |
| 5 | 0.0656 | 0.0651 | 0.7361 |
| 7 | 0.0473 | 0.0470 | 0.7610 |
| 9 | 0.0370 | 0.0367 | 0.7942 |
| 11 | 0.0303 | 0.0301 | 0.8356 |
| 13 | 0.0257 | 0.0255 | 0.8854 |

## A-3 P+CL controller

A P+CL controller is simulated in open loop. A P+CL controller is a PI controller, but then the linear integrator is replaced with the Clegg integrator. This controller needs a feed through matrix $D$ to describe its behavior. Its controller structure is given in Figure A-3, and its equation by Eq. (A-4).

$$R(s) = \frac{s+1}{s} \tag{A-4}$$

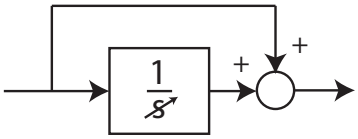


**Figure A-3:** Overview of a P+CL controller

**Table A-3:** Comparison of FFT results with HOSIDF for P+CL control

| Order | FFT Mag | HOSIDF Mag | Error in % |
|---|---|---|---|
| 1 | 1.7090 | 1.7113 | 0.1315 |
| 3 | 0.2123 | 0.2122 | 0.0353 |
| 5 | 0.1275 | 0.1273 | 0.1012 |
| 7 | 0.0911 | 0.0909 | 0.2001 |
| 9 | 0.0710 | 0.0707 | 0.3322 |
| 11 | 0.0582 | 0.0579 | 0.4976 |
| 13 | 0.0493 | 0.0490 | 0.6967 |

## A-4 Partial Clegg integrator

The Clegg integrator is simulated in open loop again, but now with it will not reset to zero, but to a fraction of its current state. The reset matrix is $A_r = 0.4$.

$$R(s) = \frac{1}{s} \qquad A_r = 0.4 \tag{A-5}$$

**Table A-4:** Comparison of FFT results with HOSIDF for a partial Clegg integrator

| Order | FFT Mag | HOSIDF Mag | Error in % |
|---|---|---|---|
| 1 | 0.1134 | 0.1139 | 0.4852 |
| 3 | 0.0182 | 0.0182 | 0.1314 |
| 5 | 0.0109 | 0.0109 | 0.1973 |
| 7 | 0.0078 | 0.0078 | 0.2963 |
| 9 | 0.0061 | 0.0061 | 0.4285 |
| 11 | 0.0050 | 0.0050 | 0.5941 |
| 13 | 0.0042 | 0.0042 | 0.7933 |

## A-5 Clegg integrator with plant

A Clegg integrator $R(s)$ controlling a plant $P(s)$ in simulated in open loop.

$$R(s) = \frac{1}{\not{s}} \qquad P(s) = \frac{2s+3}{s^2+2s+3} \tag{A-6}$$

**Table A-5:** Comparison of FFT results with HOSIDF for Clegg integrator controlling a plant

| Order | FFT Mag | HOSIDF Mag | Error in % |
|---|---|---|---|
| 1 | 0.0331 | 0.0331 | 0.1415 |
| 3 | 0.0028 | 0.0028 | 0.0616 |
| 5 | 0.0010 | 0.0010 | 0.1731 |
| 7 | 0.0005 | 0.0005 | 0.3407 |
| 9 | 0.0003 | 0.0003 | 0.5649 |
| 11 | 0.0002 | 0.0002 | 0.8464 |
| 13 | 0.0002 | 0.0002 | 1.1858 |

# Appendix B

# Combined HOSIDF for the Clegg integrator

## B-1 Combined magnitude for Clegg integrator

### B-1-1 Graphical proof

Consider a Clegg integrator which is excited to a sine wave of frequency $\omega$ (see Figure B-1). The output has a jump when the input goes through zero, which happens at $t = k\frac{\pi}{\omega}$ for k=0,1,2,...

When calculating the power of a signal, the integral is calculated for the squared signal. Because the signal is squared, its negative content will become positive. The sine wave and the Clegg integrator have a symmetric response, the absolute value of the both the input and output are the same before and after $t = \frac{\pi}{\omega}$. Because of this symmetry, it is sufficient to look at the power of half a period.

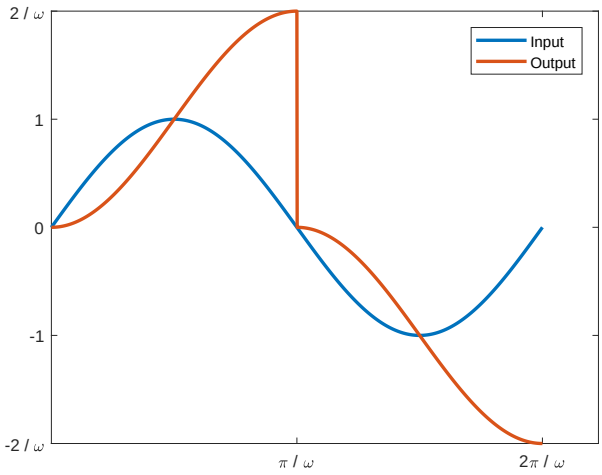


**Figure B-1:** Clegg integrator output subjected to a sinusoidal input

The output of a Clegg integrator can be described with $y(t) = \frac{1}{\omega}(1-cos(\omega t))$ when $0 < t < \frac{\pi}{\omega}$. The power of the output signal is calculated as follows:

$$Y_{pwr}(t) = \frac{\omega}{\pi}\int_0^{\frac{\pi}{\omega}} \left(\frac{1}{\omega}(1-cos(\omega t))\right)^2 dt = \frac{3}{2\omega^2} \tag{B-1}$$

When calculating this back to a corresponding amplitude:

$$A_y = \sqrt{2P_y} = \sqrt{\frac{3}{\omega^2}} \tag{B-2}$$

When a sine wave of 1 rad/s and amplitude 1 is applied, the power theory results in an amplitude of $\sqrt{3}$.

$$G_{pwr} = \frac{A_y}{A_u} = \sqrt{3} \tag{B-3}$$

### B-1-2 Mathematical proof

In the previous section, the power of a Clegg integrator was calculated by a graphical approach. In this section, the same will be proven, but now the HOSIDF will be used. The output of a reset system can be described by a summation of harmonics. The amplitudes of the harmonics can be calculated by taking the absolute values of the complex numbers, which can be calculated by the HOSIDF. In Eq. (B-4) the HOSIDF equations are shown for the Clegg integrator. When the amplitudes are known, these can be plugged in Eq. (6-7) to get the amplitude for the combined magnitude. In this section, the combined magnitude is calculated for an input frequency of 1 rad/s.

$$\begin{aligned} \text{for } n = 1 \qquad & CI(\omega) = \frac{1}{j\omega}(1 + j\frac{4}{\pi}) \\ \text{for odd n} \geq 2 \qquad & CI(\omega) = \frac{4}{\pi\omega n} \end{aligned} \tag{B-4}$$

$$\begin{aligned} \text{for } n = 1 \qquad & A_1(\omega = 1) = \left|\frac{1}{j}(1 + j\frac{4}{\pi})\right| = \sqrt{1 + \frac{4^2}{\pi^2}} \\ \text{for odd } n \geq 2 \qquad & A_n(\omega = 1) = \left|\frac{4}{\pi n}\right| = \frac{4}{\pi n} \end{aligned} \tag{B-5}$$

The squared amplitudes needs to be summed up. Because every higher harmonic is of lower amplitude, they will reach an asymptote. This asymptote can be calculated by a series. Only odd harmonics appear in the output, so we have to sum $(2n + 1)$ for $n = 1$ until $n = \infty$.

$$\sum_{n=1}^{\infty} A_{2n+1}^2 = \frac{4^2}{\pi^2} \sum_{n=1}^{\infty} (2n + 1)^{-2} = \frac{4^2}{\pi^2} \left(\frac{\pi^2}{8} - 1\right) \tag{B-6}$$

When all the squared amplitudes are added up, the following expression will form:

$$A_1^2 + A_3^2 + A_5^2 + ... = 1 + \frac{4^2}{\pi^2} + \frac{4^2\pi^2}{8\pi^2} - \frac{4^2}{\pi^2} = 3 \tag{B-7}$$

The power was however defined as the square root of this summation, so the end result will be $\sqrt{3}$.

## B-2 Combined phase for Clegg integrator

The combined phase of the Clegg integrator is the same for all frequencies. To calculate its exact value, $\omega = 1$ rad/s is plugged in to simplify the calculation.

$$\phi_c(1) = cos^{-1}\left(\frac{A_1(1)}{\sqrt{A_1^2(1) + A_3^2(1) + A_5^2(1) + ...}}\, cos(\phi_1(1))\right) \tag{B-8}$$

With

$$A_1(1) = \sqrt{(-1)^2 + \left(\frac{4}{\pi}\right)^2} \tag{B-9}$$

$$cos(\phi_1(1)) = cos\left(tan^{-1}\left(\frac{-1}{4/\pi}\right)\right) = cos\left(tan^{-1}\left(\frac{-\pi}{4}\right)\right) = \frac{4}{\sqrt{(-\pi)^2 + 4^2}} \tag{B-10}$$

This last line is better explained by Figure B-2. When an arctangent is calculated, an angle will be the result, because $\phi = tan^{-1}\left(\frac{o}{a}\right)$. We calculate the artangens for $\frac{-\pi}{4}$, so the opposite side is $o = -\pi$ and the adjacent side is $a = 4$. This makes hypotenuse side $h = \sqrt{a^2 + o^2}$. The $cos$ of the angle $\phi$ can be calculated as $cos(\phi) = \frac{a}{h} = \frac{a}{\sqrt{a^2 + o^2}}$

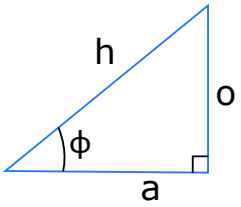


**Figure B-2:** Angle calculation of a right-angled triangle

In Eq. (B-6) it was calculated that

$$A_1^2(1) + A_3^2(1) + A_5^2(1) + ... = 3 \tag{B-11}$$

Combining these parts results in

$$\phi(1) = cos^{-1}\Big(\frac{\sqrt{1+\frac{16}{\pi^2}}}{\sqrt{3}}\frac{4}{\sqrt{\pi^2+16}}\Big) = cos^{-1}\Big(\frac{4}{\sqrt{3}}\frac{\sqrt{\pi^2+16}}{\sqrt{\pi^2(\pi^2+16)}}\Big) = cos^{-1}\Big(\frac{4}{\pi\sqrt{3}}\Big) \approx 42.68° \tag{B-12}$$

It is seen that the resulting phase is positive. Applying Algorithm 1 makes the phase negative.

# Appendix C

# MATLAB Code of the HOSIDF

In this appendix, MATLAB code is given to calculate the HOSIDF. With hosidfcalc.m, the frequency response is returned per harmonic. With hosidf.m, the HOSIDF of a reset system is plotted. With hosidfol.m, the open loop HOSIDF of a reset system and a plant is plotted.

## C-1 hosidfcalc.m

```
function [G] = hosidfcalc(sys, Ar, n, freqs)
    % G = hosidfcalc(SYS, AR, N, FREQS, CLOL)
    % Calculated the higher order (n) describing function for a reset system.
    %
    % SYS is the reset element described in state space
    % AR is the amount of reset you want to achieve (typical 0)
    % N is the describing function order
    % FREQS contains the frequencies the describing function is calculated for

    % Kars Heinen - TU Delft - 2018

    % to do; replace inv() by 'matlab \' for faster results

    % odd orders will be skipped
    if (mod(n,2) == 0)
        G = 0;
        return;
    end

    A = sys.a; B = sys.b; C = sys.c; D = sys.d;

    G = zeros(1,numel(freqs));

    for i=1:numel(freqs)
        w = freqs(i);

        Lambda = w*w*eye(size(A)) + A^2;
        LambdaInv = inv(Lambda);
```

```
        Delta = eye(size(A)) + expm(A*pi/w);
        DeltaR = eye(size(A)) + Ar*expm(A*pi/w);

        GammaR = inv(DeltaR)*Ar*Delta*LambdaInv;

        ThetaD = (-2*w*w/pi)*Delta*(GammaR-LambdaInv);

        if (n==1)
            G(i) = C*inv(j*w*eye(size(A)) - A)*(eye(size(A)) + j*ThetaD)*B;
        else
            % J1 and J2 dissappear
            G(i) = C*inv(j*w*n*eye(size(A)) - A)*j*ThetaD*B;
        end
    end

    if (n == 1)
        G = G + D;
    end
 end
```

## C-2 hosidf.m

```
function hosidf(sys, Ar, n, freqs)
    % Plots the HOSIDF of a given reset system
    % Basically a wrapper function around hosidfcalc() to actually plot stuff
    % HOSIDF(SYS, Ar, N, FREQS, CLOL)
    % SYS is the reset system in state space
    % Ar is the reset matrix (typical 0)
    % N are the orders to display (note: even orders will be skipped since they
        result in zero anyway)
    % FREQS are the frequencies to show

    % Kars Heinen - TU Delft - 2018

    % how many inputs are given
    switch nargin
        case 0
            sys = ss(-10,10,1,0); % standaard een 10/(s+10) doen
            Ar = 0;
            n = 1:2:13;
            freqs = logspace(-2,3,1000);
        case 1
            Ar = 0;
            n = 1:2:13;
            freqs = logspace(-2,3,1000);
        case 2
            n = 1:2:13;
            freqs = logspace(-2,3,1000);
        case 3
            freqs = logspace(-2,3,1000);
    end


    % freq vector contains frequency of <= 0?
    if (numel(freqs(freqs<=0)) > 0)
```

```
    error('FREQS should not contain a number <= 0! ');
end

% only odd order are accepted
n = n(mod(n,2) == 1);

% title generator
if (numel(sys.A) > 1)
    plottitle = 'HOSIDF of higher order sys';
else
    plottitle = sprintf('HOSIDF of (%d, %d, %d, %d)', sys.A, sys.B, sys.C,
        sys.D);
end

% ok finally the real function; hic sunt dracones
figure;
legendInfo = [];

Gabs = [];
Gphase = [];

for i=1:numel(n)
    order = n(i);

    L = hosidfcalc(sys, Ar, order, freqs);

    Gabs(i,:) = mag2db(abs(L));
    Gphase(i,:) = unwrap(rad2deg(phase(L)));

    legendInfo{i} = ['order ' num2str(order)];
end

GabsMag = db2mag(Gabs);

% calculate combined magnitude
GabsCombined = mag2db(sqrt(sum(GabsMag.^2,1)));

% calculate combined phase
ampPhase = GabsMag(1,:)./sqrt(sum(GabsMag.^2,1));
GphaseCombined = acosd(ampPhase .* cosd(Gphase(1,:)));

% combined phase algorithm quadrant compensation
for i=1:numel(Gphase(1,:))
    b = floor(Gphase(1,i)/180);

    if (mod(b,2)) % not divisble by 2
        GphaseCombined(i) = 180*(b+1) - GphaseCombined(i);
    else % divisble by 2
        GphaseCombined(i) = 180*b + GphaseCombined(i);
    end
end


% plot
ax1 = subplot(2,1,1);
semilogx(freqs, Gabs, 'lineWidth', 2); hold on;
semilogx(freqs, GabsCombined, 'lineWidth', 2, 'Color', 'black'); hold off;
```

```
    legendInfo{numel(n)+1} = 'Combined';

    title(plottitle);
    legend(legendInfo);
    ylabel('Magnitude [dB]');

    ax2 = subplot(2,1,2);
    semilogx(freqs, Gphase, 'lineWidth', 2); hold on;
    semilogx(freqs, GphaseCombined, 'lineWidth', 2, 'Color', 'black'); hold off
        ;

    ylabel('Phase [deg]');
    xlabel('Input frequency [rad/s]');
    linkaxes([ax1,ax2], 'x')
end
```

## C-3 hosidfol.m

```
function hosidfol(sysC, sysP, Ar, n, freqs)
    % Plots the HOSIDF of a open loop system with reset controller C and plant
        P
    % HOSIDFOL(SYSC, SYSP, Ar, N, FREQS)
    % SYSC is the reset system in state space
    % SYSP is the plant
    % Ar is the reset matrix (typical 0)
    % N are the orders to display (note: even orders will be skipped since they
         are zero)
    % FREQS are the frequencies to show

    % Kars Heinen - TU Delft - 2018

    % how many inputs are given
    switch nargin
        case 0
            sysC = ss(0,1,1,0); % example commonly used
            sysP = tf([1 1],[1 0.2 0]);
            Ar = 0;
            n = 1:2:13;
            freqs = logspace(-2,3,1000);
        case 1
            sysP = tf([1 1],[1 0.2 0]);
            Ar = 0;
            n = 1:2:13;
            freqs = logspace(-2,3,1000);
        case 2
            Ar = 0;
            n = 1:2:13;
            freqs = logspace(-2,3,1000);
        case 3
            n = 1:2:13;
            freqs = logspace(-2,3,1000);
        case 4
            freqs = logspace(-2,3,1000);
    end
```

```
% freq vector contains frequency of <= 0?
if (numel(freqs(freqs<=0)) > 0)
    error('FREQS should not contain a number <= 0! ');
end

% only odd order are accepted
n = n(mod(n,2) == 1);

% title generator
plottitle = 'HOSIDF of open loop';

% ok finally the real function; hic sunt dracones
figure;
legendInfo = {zeros(1,numel(n)+1)};

Gabs = zeros(numel(n), numel(freqs));
Gphase = zeros(numel(n), numel(freqs));

for i=1:numel(n)
    order = n(i);

    [mag, angle] = bode(sysP, freqs*order);
    absP = mag2db(squeeze(mag)');
    angleP = squeeze(angle)';

    C = hosidfcalc(sysC, Ar, order, freqs);
    absC = mag2db(abs(C));
    angleC = rad2deg(phase(C));

    % do not convert to complex number and add, because the phase will wrap
    Gabs(i,:) = absP + absC;
    Gphase(i,:) = angleP + angleC;

    legendInfo{i} = ['order ' num2str(order)];
end


GabsMag = db2mag(Gabs);

% calculate combined magnitude
GabsCombined = mag2db(sqrt(sum(GabsMag.^2,1)));

% calculate combined phase
ampPhase = GabsMag(1,:)./sqrt(sum(GabsMag.^2,1));
GphaseCombined = acosd(ampPhase .* cosd(Gphase(1,:)));

% combined phase algorithm quadrant compensation
for i=1:numel(Gphase(1,:))
    b = floor(Gphase(1,i)/180);

    if (mod(b,2)) % not divisble by 2
        GphaseCombined(i) = 180*(b+1) - GphaseCombined(i);
    else % divisble by 2
        GphaseCombined(i) = 180*b + GphaseCombined(i);
    end
end
```

```
    % draw plot
    ax1 = subplot(2,1,1);
    semilogx(freqs, Gabs, 'lineWidth', 2); hold on;
    semilogx(freqs, GabsCombined, 'lineWidth', 2, 'Color', 'black'); hold off;

    title(plottitle);
    ylabel('Magnitude [dB]');

    ax2 = subplot(2,1,2);
    semilogx(freqs, Gphase, 'lineWidth', 2); hold on;
    semilogx(freqs, GphaseCombined, 'lineWidth', 2, 'Color', 'black'); hold off
        ;

    ylabel('Phase [deg]');
    xlabel('Input frequency [rad/s]');
    linkaxes([ax1,ax2], 'x');

    legendInfo{numel(n)+1} = 'Combined';
    legend(legendInfo);
end
```

# Bibliography


[1] G. Stein, "Respect the unstable," *IEEE Control Systems*, vol. 23, pp. 12–25, Aug 2003.

[2] A. Baños and A. Barreiro, *Reset Control Systems*. Springer, 2012.

[3] P. Nuij, O. Bosgra, and M. Steinbuch, "Higher-order sinusoidal input describing functions for the analysis of non-linear systems with harmonic responses," *Mechanical Systems and Signal Processing*, vol. 20, no. 8, pp. 1883 – 1904, 2006.

[4] K. Åström and T. Hägglund, "The future of pid control," *Control Engineering Practice*, vol. 9, no. 11, pp. 1163 – 1175, 2001. PID Control.

[5] M. Heertjes and M. Steinbuch, "Stability and performance of a variable gain controller with application to a dvd storage drive," *Automatica*, vol. 40, no. 4, pp. 591 – 602, 2004.

[6] W. Aangenent, R. van de Molengraft, and M. Steinbuch, "Nonlinear control of a linear motion system," *IFAC Proceedings Volumes*, vol. 38, no. 1, pp. 446 – 451, 2005. 16th IFAC World Congress.

[7] J. C. Clegg, "A nonlinear integrator for servomechanisms," *Transactions of the American Institute of Electrical Engineers, Part II: Applications and Industry*, vol. 77, pp. 41–42, March 1958.

[8] K. Aström and R. Murray, *Feedback Systems: An Introduction for Scientists and Engineers*. Princeton University Press, 2010.

[9] Y. Chait and C. Hollot, "On horowitz's contributions to reset control," vol. 12, pp. 335 – 355, 04 2002.

[10] Y. Guo, Y. Wang, and L. Xie, "Frequency-domain properties of reset systems with application in hard-disk-drive systems," *IEEE Transactions on Control Systems Technology*, vol. 17, pp. 1446–1453, Nov 2009.

[11] M. A. Davó and A. Baños, "Reset control of a liquid level process," in *2013 IEEE 18th Conference on Emerging Technologies Factory Automation (ETFA)*, pp. 1–4, Sept 2013.

[12] A. Vidal and B. Alfonso., *Reset Compensation for Temperature Control: Experimental Application on Heat Exchangers.* Chemical Engineering Journal, 2010.

[13] J. Freudenberg, R. Middleton, and A. Stefanpoulou, "A survey of inherent design limitations," in *Proceedings of the 2000 American Control Conference. ACC (IEEE Cat. No.00CH36334)*, vol. 5, pp. 2987–3001 vol.5, 2000.

[14] M. Ivens, "Robust reset control: using adaptive/iterative learning control," Master's thesis, TU Delft, the Netherlands, 2018.

[15] M. F. Y. W. J. Zheng, Y. Guo and L. Xie., *Improved Reset Control Design for a PZT Positioning Stage.* 2007 IEEE International Conference on Control Applications, 2007.

[16] Y. G. et al., *Optimal Reset Law Design of Reset Control Systems with Application to Hdd Systems.* Proceedings of the Ieee Conference on Decision and Control, 2009.

[17] A. Banos and A. Vidal, *Definition and tuning of a PI+CI reset controller.* 2007 European Control Conference (ECC), 2007.

[18] S. van Loon, K. Gruntjens, M. Heertjes, N. van de Wouw, and W. Heemels, "Frequency-domain tools for stability analysis of reset control systems," *Automatica*, vol. 82, pp. 101–108, 2017.

[19] Q. Chen, C. V. Hollot, and Y. Chait, "Stability and asymptotic performance analysis of a class of reset control systems," in *Proceedings of the 39th IEEE Conference on Decision and Control (Cat. No.00CH37187)*, vol. 1, pp. 251–256 vol.1, 2000.

[20] H. Hu, Y. Zheng, Y. Chait, and C. V. Hollot, "On the zero-input stability of control systems with clegg integrators," in *Proceedings of the 1997 American Control Conference (Cat. No.97CH36041)*, vol. 1, pp. 408–410 vol.1, Jun 1997.

[21] M. Vidyasagar, *Nonlinear Systems Analysis.* Prentice Hall, 1993.

[22] R. S. Barbosa, J. T. Machado, and I. M. Ferreira, "Describing function analysis of mechanical systems with nonlinear friction and backlash phenomena," *IFAC Proceedings Volumes*, vol. 36, no. 2, pp. 269 – 274, 2003. 2nd IFAC Workshop on Lagrangian and Hamiltonian Methods for Nonlinear Control 2003, Seville, Spain, 3-5 April 2003.

[23] A. Besançon-Voda and P. Blaha, "Describing function approximation of a two-relay system configuration with application to coulomb friction identification," *Control Engineering Practice*, vol. 10, no. 6, pp. 655 – 668, 2002.

[24] D. Rijlaarsdam, P. Nuij, J. Schoukens, and M. Steinbuch, "A comparative overview of frequency domain methods for nonlinear systems," *Mechatronics*, vol. 42, pp. 11 – 24, 2017.

[25] A. Gelb and W. E. V. Velde., *Multiple-Input Describing Functions and Nonlinear System Design.* McGraw-Hill, 1968.

[26] M. Román and E. Ponce, "The describing function method accuracy in first order plants with rate-limited feedback," in *2003 European Control Conference (ECC)*, pp. 1620–1625, Sept 2003.

[27] L. Ucun and J. Salášek, "Hosidf-based feedforward friction compensation in low-velocity motion control systems," *Mechatronics*, vol. 24, no. 2, pp. 118 – 127, 2014.

[28] P. Nuij, M. Steinbuch, and O. Bosgra, "Measuring the higher order sinusoidal input describing functions of a non-linear plant operating in feedback," *Control Engineering Practice*, vol. 16, no. 1, pp. 101 – 113, 2008.

[29] R. Munnig Schmidt, G. Schitter, A. Rankers, and J. van Eijk, *The design of high performance mechatronics: high-tech functionality by multidisciplinary system integration (2nd revised edition)*. Netherlands: IOS Press, 2014. NEO.

[30] D. Brandwood, *Fourier Transforms in Radar and Signal Processing*. Artech House radar library, Artech House, 2003.